JOURNAL OF PROPULSION AND POWER
Vol. 22, No. 2, March–April 2006

Turbine Blade Internal Cooling Passages with Rib Turbulators

Je-Chin Han and Hamn-Ching Chen
Texas A&M University, College Station, Texas 77843-3123

Gas turbines are extensively used for aircraft propulsion, land-based power generation, and industrial applications. Developments in turbine cooling technology play a critical role in increasing the thermal efficiency and power output of advanced gas turbines. Gas turbine blades are cooled internally by passing the coolant through several rib-enhanced serpentine passages to remove heat conducted from the outside surface. For internal cooling, focus is placed on the effect of rotation on rotor blade coolant passage heat transfer with rib turbulators. In particular, the most recent publications are covered that deal with the rotational effects on internal cooling passage heat transfer with low and high aspect ratio channels with various high-performance rib geometries. To better understand the complex three-dimensional flow physics in the complicated blade internal coolant passage geometry, the computational flow and heat transfer results are presented and compared using the Reynolds averaged Navier–Stokes method with various turbulence models such as k–ε, and second-moment closure models.

Nomenclature

AR	=	channel aspect ratio
D_h	=	hydraulic diameter
e	=	rib height
h	=	heat transfer coefficient
k	=	thermal conductivity of coolant
Nu	=	local Nusselt number, hD/k
Nu_0	=	Nusselt number in fully-developed turbulent non-rotating tube flow, hD/k
P	=	rib pitch
Pr	=	Prandtl number
Re	=	Reynolds number, $\rho W_b D_h/\mu$
Ro	=	rotation number, $\Omega D_h/W_b$
R_r	=	radius from axis of rotation
T	=	local coolant temperature
T_w	=	local wall temperature
T_0	=	coolant temperature at inlet
W_b	=	bulk velocity in streamwise direction
α	=	rib angle
β	=	channel orientation measured from direction of rotation
$\Delta\rho/\rho$	=	inlet coolant-to-wall density ratio, $(T_w - T_0)/T_w$
θ	=	dimensionless temperature, $(T - T_0)/(T_w - T_0)$
μ	=	dynamic viscosity of coolant
ρ	=	density of coolant
Ω	=	rotational speed

Introduction

ADVANCED gas turbine engines operate at high temperatures (1200–1500°C) to improve thermal efficiency and power output. As the turbine inlet temperature increases, the heat transferred to the turbine blade also increases. The level and variation in the temperature within the blade material, which cause thermal stresses, must be limited to achieve reasonable durability goals. The operating temperatures are far above the permissible metal temperatures. Therefore, there is a critical need to cool the blades for safe operation. The blades are cooled with extracted air from the compressor of the engine. Because this extraction incurs a penalty on the thermal efficiency and power output of the engine, it is important to understand and optimize the cooling technology for a given turbine blade geometry under engine operating conditions. Gas turbine cooling technology is complex and varies between engine manufacturers. Figure 1 shows the common cooling technology with three major internal cooling zones in a turbine blade with strategic film cooling in the leading edge, pressure and suction surfaces, and blade tip region. The leading edge is cooled by jet impingement with film cooling, the middle portion is cooled by serpentine rib-roughened passages with local film cooling, and the trailing edge is cooled by pin fins with trailing-edge injection. This paper focuses on the rotational effects on the turbine blade internal cooling passage heat transfer with rib turbulators. Several recent publications address state-of-the-art reviews of turbine blade cooling and heat transfer. These include a

---

Je-Chin Han, Marcus C. Easterling Chair, Professor of Mechanical Engineering at Texas A&M University has been working on gas turbine blade internal cooling, heat transfer in rotating flows, and film cooling in unsteady high turbulent flows for more than 25 years. He served as an Associate Technical Editor for ASME *Journal of Heat Transfer* (1997-2000). He is currently an Associate Technical Editor for AIAA *Journal of Thermophysics and Heat Transfer*, ASME *Journal of Turbomachinery*, and an Associate Editor-in-Chief for *International Journal of Rotating Machinery*. He is currently the Chair for ASME K-14 Gas Turbine Heat Transfer Committee (2004–2006). He is the recipient of the ASME Heat Transfer Memorial Award (2002), the AIAA Thermophysics Award (2004), and the International Symposium in Rotating Machinery Award (2004). He is author or coauthor of over 150 papers in archival journals and a book on gas turbine heat transfer and cooling technology.

Hamn-Ching Chen, Professor of Civil Engineering and of Ocean Engineering at Texas A&M University received his Ph.D. in Mechanical Engineering from the University of Iowa in 1982. After working as a research scientist at the Iowa Institute of Hydraulic Research (1982–1988) and a senior research scientist at Science Applications International Corporation (1988–1990), he joined the faculty of Texas A&M University in 1991, where he was promoted to Professor in 2001. His research interests include computational fluid dynamics, turbulence modeling, internal cooling and film cooling of turbine blades, ship and submarine hydrodynamics, vortex-induced vibrations, and bridge scour. He served as Chair of ASCE Turbulence Committee and an Associate Editor for *Journal of Engineering Mechanics* in 2000–2002. He is currently an Associate Editor for ASCE *Journal of Waterway, Port, Coastal and Ocean Engineering*. He is author or coauthor of over 50 papers in archival journals.

Received 11 August 2004; accepted for publication 31 January 2005.

study on rotational effect on the turbine blade coolant passage heat transfer by Dutta and Han,[1] recent studies in turbine blade cooling by Han,[2] and recent developments in turbine blade internal cooling by Han and Dutta.[3] A recent book focusing entirely on the range of gas turbine heat transfer issues and the associated cooling technology is available by Han et al.[4] A symposium volume dealing with heat transfer in gas turbine systems was recently edited by Goldstein.[5] A detailed review of convective heat transfer and aerodynamics in axial flow turbines is available by Dunn.[6]

Coolant Passage Heat Transfer with Rib Turbulators

In advanced gas turbine blades, rib turbulators are often cast on two opposite walls of internal coolant passages to augment heat transfer. The internal coolant passages are mostly modeled as short, square or rectangular channels with various aspect ratios. The heat transfer augmentation in rectangular coolant passages with rib turbulators primarily depends on the rib turbulators' geometry, such as rib size, shape, distribution, and flow attack angle, and the flow Reynolds number. Rib turbulators disturb only the near-wall flow for heat transfer enhancement. Therefore, the pressure drop penalty caused by rib turbulators is affordable for the blade internal cooling designs. There have been many basic studies (Refs. 7–12) to understand the heat transfer augmentation vs the pressure drop penalty by the flow separation–reattachment caused by rib-turbulators for symmetric (parallel) rib arrangements in opposite walls of a cooling channel. The heat transfer coefficients can be further enhanced by casting the ribs with an angle to the coolant flow, which causes a rib-induced secondary flow moving in the rib angle direction, as seen in Fig. 2. The Reynolds numbers based on coolant channel hydraulic diameter vary from 1×10^4 to 8×10^4 in the aircraft engine turbine blades. However, the Reynolds numbers can be up to 5×10^5 for the coolant passages in large power generation turbine blades. In general, the repeated ribs that used for coolant passages with a channel aspect ratio varying from one-fourth (near blade leading edge) to four (near blade trailing edge) are nearly square in cross section with a typical relative rib height of 5–10% of the coolant channel hydraulic diameter, a rib spacing-to-height ratio varying from 5 to 15, and a rib flow attack angle around 30–60 deg.

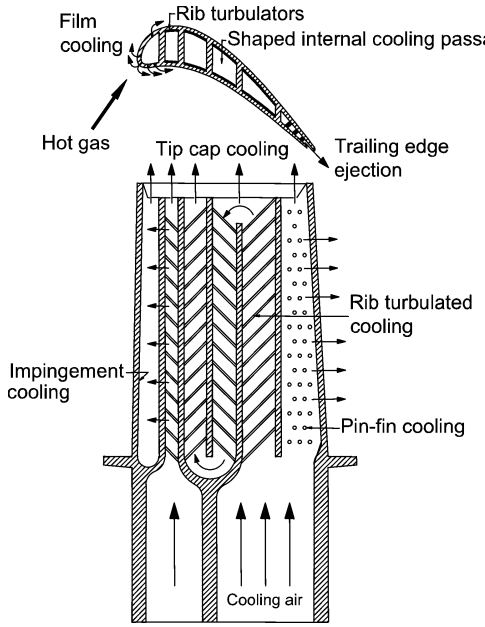

Fig. 1 Schematic of modern gas turbine blade with typical internal cooling techniques.

In general, smaller rib height is more efficient for higher Reynolds number flows, and the heat transfer enhancement decreases but pressure drop penalty increases with the Reynolds number. For example, the heat transfer can be enhanced about three times with five times pressure drop penalty in a square channel with typical rib geometry (6% rib height-to-channel hydraulic diameter ratio, 10 rib spacing-to-height ratio, and 45-deg rib flow attack angle) at a Reynolds number around 3×10^4. Several studies by Han and Zhang,[13] Han et al.[14] and Ekkad et al.[15] show that the V-shaped and delta-shaped ribs provide better heat transfer performance than the typical angled rib geometry for a given pressure drop penalty due to secondary flow vortices induced by angled ribs and V-shaped ribs (Fig. 2). However, larger rib height-to-channel hydraulic diameter ratio can be used to generate a little more heat transfer enhancement if the pressure drop penalty is not a main concern in some highly demanding cooling designs. Also, the closer (or wider) rib spacing has reduced

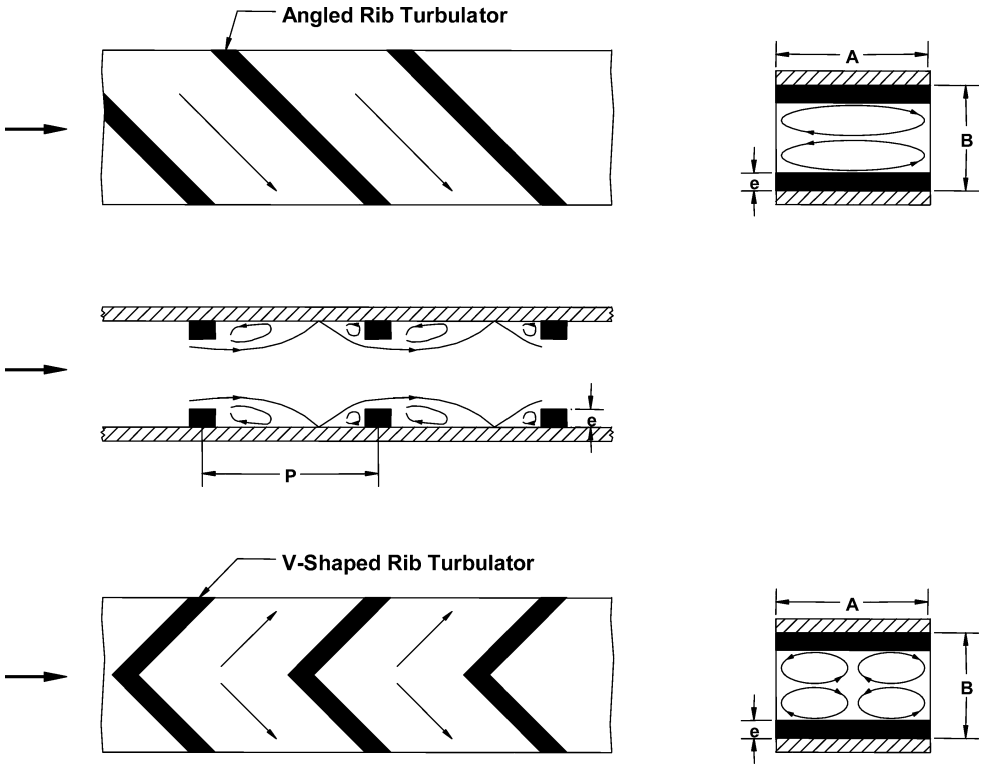

Fig. 2 Angled and V-shaped rib-induced secondary flow.

heat transfer enhancement and pressure drop penalty. Therefore, the closer (or wider) rib spacing can be used to get enough heat transfer enhancement if the pressure drop penalty is a major concern in certain cooling designs. In these cases, the closer rib spacing can be used due to the increased rib-side area for convection (fin effect), in addition to the heat transfer enhancement. For example, smaller gas turbine blades have larger blockage ribs with 10–20% rib height-to-hydraulic diameter ratio at closer spacing with 5 rib spacing-to-height ratio reported by Taslim and Wadsworth[16] and Taslim and Lengkong.[17,18]

Effects of Rotation on Coolant Passage Heat Transfer

Rotational Effect on Internal Cooling

Rotation induces Coriolis and centrifugal forces that produce cross-stream secondary flow in the rotating coolant passages; therefore, heat transfer coefficients in rotor coolant passages are very much different from those in nonrotating frames. Figure 3 shows a schematic of the secondary flow and axial flow distribution in a rotating two-pass square channel. One important finding from recent studies is that rotation can greatly enhance heat transfer on one side of the cooling channel and reduce heat transfer on the opposite side of the cooling channel due to rotating-induced secondary flow, depending on the radial outflow or inflow of the cooling passages. Without considering the rotational effect, the coolant passage would be overcooled on one side while overheated on the opposite side. Recent studies focus on the combined effects of rotation, channel shape, orientation, and aspect ratio on rotor coolant passage heat transfer with various high-performance rib turbulators. Results show that the channel shape, orientation, and aspect ratio significantly change local heat transfer coefficient distributions in rotor coolant passages with rib turbulators. To better understand the complex three-dimensional flow physics in the complicated blade internal coolant passage geometry, recent efforts also focus on the computational flow and heat transfer using the Reynolds averaged Navier–Stokes (RANS) method with various turbulence models. Results indicate that the second-moment turbulence closure model provides better flow and heat transfer predictions than the standard k–ε model. The existing and modified computational fluid dynamics (CFD) codes would become useful tools for rotor coolant passage heat transfer prediction and coolant flow optimization and management. Recent studies also focus on the effects of rotation on impingement cooling and pin-fin or dimple cooling in the blade leading-edge and trailing-edge regions, respectively. Results show that rotation creates a negative impact on rotor coolant passages with impinging jets. In general, rotation reduces the impingement cooling effect due to jet deflection away from the impinged surface. However, rotation enhances the pin-fin or dimple cooling effect due to the narrow passage orientation in the blade trailing-edge region.

Heat Transfer in Rotating Coolant Passages with Square Cross-Section

Heat transfer in rotating multipass coolant passages with square cross section and smooth walls was reported by Wagner et al.[19] Results show that the heat transfer coefficient can enhance 2–3 times on the trailing surface and reduce up to 50% on the leading surface for the first-pass radial outward flow passage; however, the reverse is true for the second-pass radial inward flow passage due to the flow direction change. Results also show that the heat transfer difference between leading and trailing surfaces is greater in the first pass than that in the second pass due to the centrifugal buoyancy opposite to the flow direction. Heat transfer in rotating multipass coolant passages with square cross section with 45-deg rib-turbulated walls was reported by Johnson et al.[20] Results show that rotation and buoyancy in general have less effect on the rib-turbulated coolant passage than on the smooth-wall coolant passage. This is because the heat transfer enhancement in the ribbed passages is already up to 3.5 times higher than in the smooth passages; therefore, the rotational effect is still important but with a reduced percentage. Results also show that, like a nonrotating channel, the 45-deg ribs perform better than 90-deg ribs and subsequently better than the smooth channel.

Wall Heating Condition Effect on Rotating Coolant Passage Heat Transfer

From the preceding analyses, the rotation effect on channel heat transfer comes from the Coriolis and centrifugal forces. The centrifugal force is known as rotation buoyancy when there is a temperature difference between the coolant and the channel walls at rotating conditions. Because the temperature difference between the coolant and the channel walls varies along the coolant passages, so does the rotation buoyancy. Therefore, it is expected that the channel wall heating conditions would affect rotor coolant passage heat transfer. The channel heating conditions imply that the channel walls may be at the same temperature (or heat flux) in both streamwise and circumferential directions, or the trailing wall temperature may be higher than the leading wall temperature in real turbine blade cooling

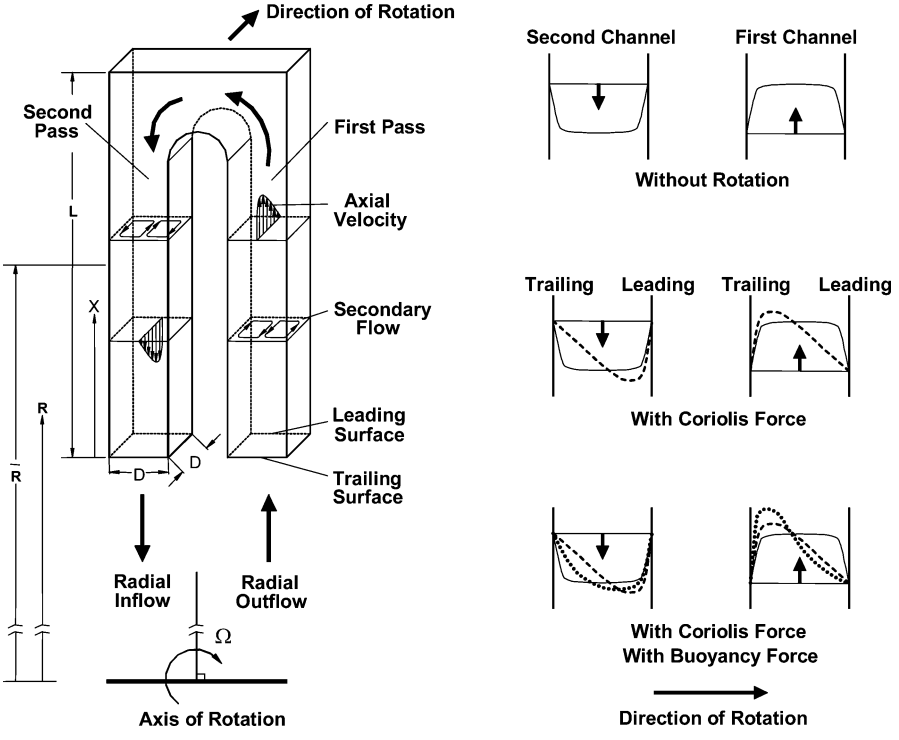

Fig. 3 Coolant flow through two-pass rotating channel.

applications. Han et al.[21] studied the uneven wall temperature effect on rotating two-pass square channels with smooth walls. They concluded that in the first pass, the local uneven wall temperature interacts with the Coriolis force-driven secondary flow and enhances the heat transfer coefficients in both leading and trailing surfaces, with a noticeable increase in the leading side, as compared with the uniform wall temperature case. However, the uneven wall temperature significantly enhances heat transfer coefficients on both leading and trailing surfaces. Parsons et al.[22] and Zhang et al.[23] studied the influence of wall heating condition on the local heat transfer coefficient in rotating two-pass square channels with 90-deg ribs and 60-deg ribs on the leading and trailing walls, respectively. They concluded that the uneven wall temperature significantly enhances heat transfer coefficients on the first-pass leading and second-pass trailing surfaces as compared with the uniform wall temperature condition.

Effect of Channel Orientation with Respect to the Rotation Direction

Because the turbine blade is curved, the rotor blade cooling passage can have different channel orientations with respect to the rotating plane. Johnson et al.[24] studied the effects of rotation on the heat transfer for smooth and 45-deg ribbed serpentine channels with channel orientations of 0 and 45 deg to the axis of rotation. They found that the effects of Coriolis and buoyancy forces on heat transfer in the rotating channel are decreased with the channel at 45 deg compared to the results at 0 deg. This implies that the difference in heat transfer coefficient between leading and trailing surfaces due to rotation will be reduced when the channel has an angle to the axis of rotation. Parsons et al.[25] used 60-deg angled ribs, Dutta and Han[26] used high-performance broken V-shaped ribs, and Al-Hadhrami and Han[27] used parallel and crossed 45-deg angled ribs in rotating two-pass square channels to study the effect of channel orientation on heat transfer. The channel orientation with respect to the rotation axis influences the secondary flow vortices induced by rotation. The secondary flow developed by broken V-shaped ribs could interact with the secondary flow of rotation, and a new flow pattern might be established. The two cell vortices induced by rotation could interact with the two cell vortices induced by the parallel 45-deg ribs and the single cell vortex induced by the crossed 45-deg ribs. They concluded that the broken V-shaped ribs are better than the 60-deg angled ribs; the parallel 45-deg angled ribs are better than the crossed 45-deg angled ribs. In general, the difference between leading and trailing wall heat transfer coefficients is reduced for the channel with a 45-deg angle to the axis of rotation.

Heat Transfer in Rotating Coolant Passages with Triangular Cross Section

Rotating coolant passages with triangular cross section might be used on some portion of the blade to provide compact channel structure and good cooling efficiency. Clifford et al.[28] studied the mean heat transfer in a straight triangular-sectioned rotating duct with smooth walls. Harasgama and Morris[29] compared the effect of rotation on heat transfer in straight circular, triangular, and square duct with smooth walls. Dutta et al.[30,31] studied the effect of rotation on the heat transfer coefficients in two-pass triangular channels with smooth and ribbed walls. For the locations in the first pass, the triangular-duct heat transfer coefficients are mostly contained within the upper and lower limits imposed by the square duct. This is because, in a triangular duct, there is less space for the coolant to form secondary flow by rotation. However, in the second pass, the leading surface of the triangular duct shows much higher heat transfer coefficients than the square duct. This is due to more mixing and favorable secondary flow in the 180-deg turn for the triangular duct geometry. They also found that channel orientation and uneven wall temperature have a significant effect on the surface heat transfer coefficient distributions.

Heat Transfer in Rotating Coolant Passages with Rectangular Cross Section

Most of the mentioned studies dealt with square channels. However, a rectangular coolant passage is of high importance to maintain the integrity of gas turbine blade internal cooling design. The curved shape of the turbine blade may prohibit the efficient use of square cross-sectional coolant flow channels. It is quite common to find rectangular cooling passages, particularly moving from the midchord to the trailing edge (or leading edge) of the blade; the channels must become more rectangular as the blade becomes thinner (or thicker) as shown in Fig. 4. This thinning (or thickening) of the channel changes the effective secondary flow pattern from that of a square duct. For this reason, one cannot simply apply the knowledge of the rotationally induced flow pattern and the associated surface heat transfer coefficients in a square channel (aspect ratio equal to 1:1 at blade midchord region) to that of a rectangular channel (higher aspect ratio equal to 2:1 and 4:1 near blade trailing edge, or lower aspect ratio equal to 1:2 and 1:4 near blade leading-edge region). However, very few experimental heat transfer data on a rectangular coolant passage are available in the literature. Guidez[32] reported the effect of rotation on heat transfer in a straight rotating rectangular channel (aspect ratio equal to 2:1) with smooth walls. Soong et al.[33] conducted heat transfer experiments in rotating smooth straight ducts with different aspect ratios ranging from 0.2 to 5.0. They concluded that the aspect ratio of the duct was a critical parameter in the secondary flow patterns. Taslim et al.[34] conducted experiments with liquid crystal to study the effect of rotation on two straight rectangular ducts (aspect ratios equal to 1:1 and 1:2) with 45-deg cross ribs. Azad et al.[35] and Al-Hadhrami et al.[36] studied heat transfer in a two-pass rectangular rotating channel (aspect ratio equal to 2:1) with 45-deg angled ribbed walls and 45-deg V-shaped ribbed walls, respectively, including the effect of channel orientation with respect to the axis of rotation. The two cell vortices induced by rotation could interact with the four cell vortices induced by 45-deg V-shaped ribs and the two cell vortices induced by 45-deg crossed V-shaped ribs. They found that the effect of rotation on the two-pass rectangular channel is very similar to that on the two-pass square channel except the leading surface heat transfer coefficient does not vary much with the rotation compared with the square channel case. The results show that 45-deg V-shaped ribs are better than 45-deg crossed V-shaped ribs and subsequently better than 45-deg parallel angled ribs. Figure 5 shows many rib configurations reported in the open literature.

Griffith et al.[37] studied heat transfer in a single-pass rectangular channel (aspect ratio equal to 4:1) with smooth and 45-deg angled

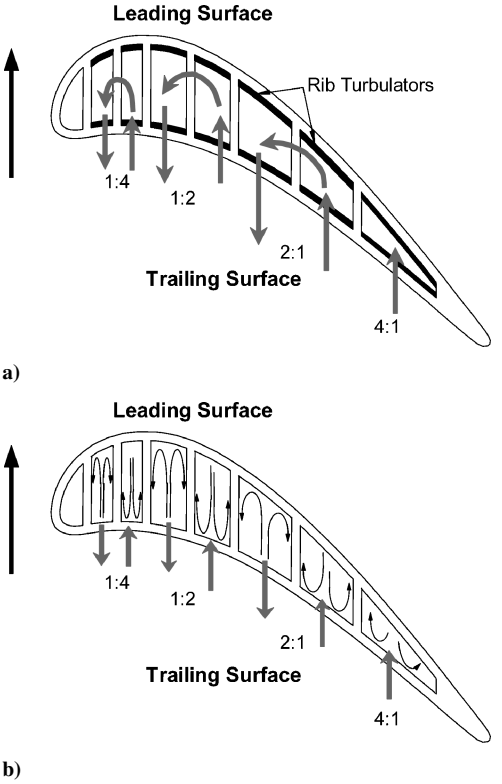

Fig. 4 Conceptual view of a rotating cooling passage: a) cooling passage size and orientation and b) rotation-induced secondary flow.

ribbed walls, including the effect of channel orientation with respect to the axis of rotation. Results show that the narrow rectangular passage exhibits a much higher heat transfer enhancement for the ribbed surface than the square and 2:1 channels previously investigated. Also, channel orientation significantly affects the leading and side surfaces, yet does not have much effect on the trailing surfaces for both smooth and ribbed surfaces. Therefore, this investigation has determined that spanwise variations in the heat transfer distribution of rectangular cooling passages exist and that the enhancement is a function of channel orientation with respect to the axis of rotation, surface configuration (such as smooth or 45-deg angled ribbed walls), and channel aspect ratio. Willett and Bergles[38] studied heat transfer in a single-pass narrow, 10:1 smooth rectangular channel oriented at an angle to the axis of rotation. They focused on the rotating buoyancy effect on local heat transfer coefficients. They found that the channel orientation induced a significant variation in the heat transfer coefficient in the spanwise direction. They also found that the heat transfer coefficient at the far aft end of the trailing surface is a very strong function of rotation buoyancy.

Lee et al.[39] studied heat transfer in a single-pass rectangular channel (aspect ratio equal to 4:1) with V-shaped and angled rib turbulators with and without gaps (Fig. 5), including the effect of channel orientation with respect to the axis of rotation. The results show that V-shaped rib configuration produces more heat transfer enhancement than the angled rib configurations for both the stationary and rotating cases. There is only negligible difference in heat transfer enhancement between the parallel and staggered rib configurations for both the stationary and rotating cases. The results also show

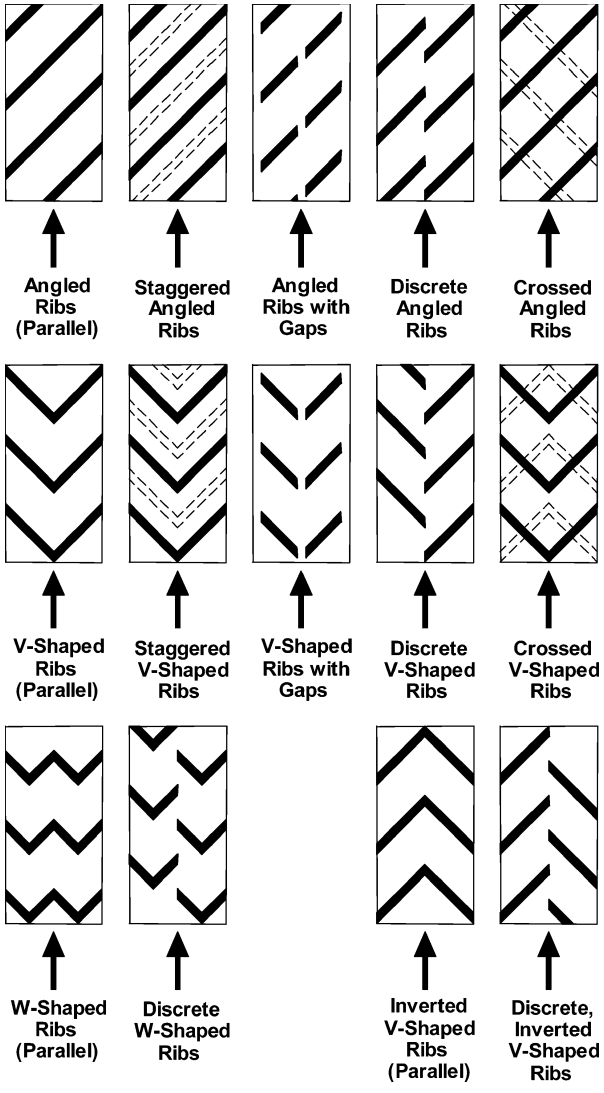

Fig. 5 Various rib configurations used to enhance internal heat transfer.

that the V-shaped ribs with gaps produce overall less heat transfer enhancement than the V-shaped ribs without gaps; whereas the angled ribs with gaps produce overall greater heat transfer enhancement than the angled ribs without gaps for the stationary case and clearly the same enhancement for the rotating case. Most important, for narrow rectangular rib-turbulated channels oriented at 135 deg with respect to the plane of rotation, heat transfer enhancement on both the leading and trailing surfaces increases with rotation. This is quite different from the square channel that rotation enhances trailing surface heat transfer but reduces the leading surface heat transfer for radial outward flow case. This provides positive information for cooling designers. Acharya et al.[40] used naphthalene sublimation to confirm these trends in a 4:1 two-pass, rotating channel. They, too, showed that in a channel oriented at 45 deg to the direction of rotation the heat transfer on all surfaces increases with rotation; however, in a 4:1 channel oriented normal to the direction of rotation, heat transfer is enhanced on the destabilized walls (first pass trailing and second pass leading) whereas it decreases on the stabilized walls (first pass leading and second pass trailing). The detailed measurements of this study also reiterate the significant spanwise variation present in these narrow channels. Zhou et al.[41] extended the studies of 4:1 channels to include high Reynolds number flow in smooth and ribbed channels at high rotation numbers. They concluded that there is a critical Reynolds number beyond which the expected heat transfer trends reverse. They also showed that increasing the density ratio increases the heat transfer enhancement. With this positive heat transfer performance, Wright et al.[42] further investigated 4:1 channels with high-performance ribs. This investigation evaluated the thermal performance of angled, V-shaped, and W-shaped ribs (Fig. 5) by measuring both the heat transfer enhancement and the pressure penalty in the ribbed channels; discrete angled, V-shaped, and W-shaped rib configurations were also compared in this study. Discrete W-shaped and discrete V-shaped ribs proved to have the greatest overall performance whereas the more standard angled ribs performed the worst in both rotating and non-rotating channels.

Agarwal et al.[43] reported the effect of rotation on heat transfer with a naphthalene sublimation technique in two-pass rectangular channels (aspect ratios equal to 1:1 and 1:4) with smooth and 90-deg ribbed walls. They concluded that the 1:4 rectangular channel provides lower levels of heat transfer enhancement along the destabilized wall and higher levels of heat transfer degradation along the stabilized wall compared to the 1:1 square channel. Cho et al.[44] studied the effect of rotation on heat transfer with a naphthalene sublimation technique in a two-pass rectangular channel (aspect ratio equal to 1:2) with smooth and 70-deg ribbed walls. That found that the effect of rotation diminishes in the radial inward channel due to strong 180-deg flow turning into the second pass of the two-pass channel. This is quite different from that found in the two-pass rectangular channels with aspect ratio greater than unity (aspect ratios equal to 1:1 and 2:1). Kim et al.[45] performed a study to compare the heat transfer enhancement due to rotation in various aspect ratio channels (aspect ratios equal to 1:2, 1:1, and 2:1) with orthogonal ribs. From their mass transfer experiments, they concluded that the heat transfer enhancement due to the rib turbulators is greatest in 2:1 channels, and this is followed by the 1:1 and 1:2 channels, respectively. Although the rib height-to-hydraulic diameter remained constant in the three channels, the ribs created more blockage in the 2:1 channel (rib height-to-channel height ratio) and thus, increased enhancement from the accelerated flow in the midsections of the ribs. They also concluded that the effect of rotation is greatest in the 1:2 channel, followed by the 1:1 and 2:1 channels, respectively. Fu et al.[46,47] performed a similar investigation for 1:2 and 1:4 two-pass channels with smooth and ribbed (45-deg) walls. Rotation increases the heat transfer on the first-pass trailing wall while reducing the heat transfer from the first-pass leading wall. However, the effect of rotation is reduced in the second pass of both aspect ratio channels, and the difference between the leading and trailing walls decreases. This trend was observed in both channels with smooth and ribbed walls.

With many investigations exploring a wide range of channel sizes, direct comparisons of multiple aspect ratio channels would be beneficial for blade designers. Figure 6 shows a summary of the heat transfer enhancement in rotating channels (smooth or ribbed walls)

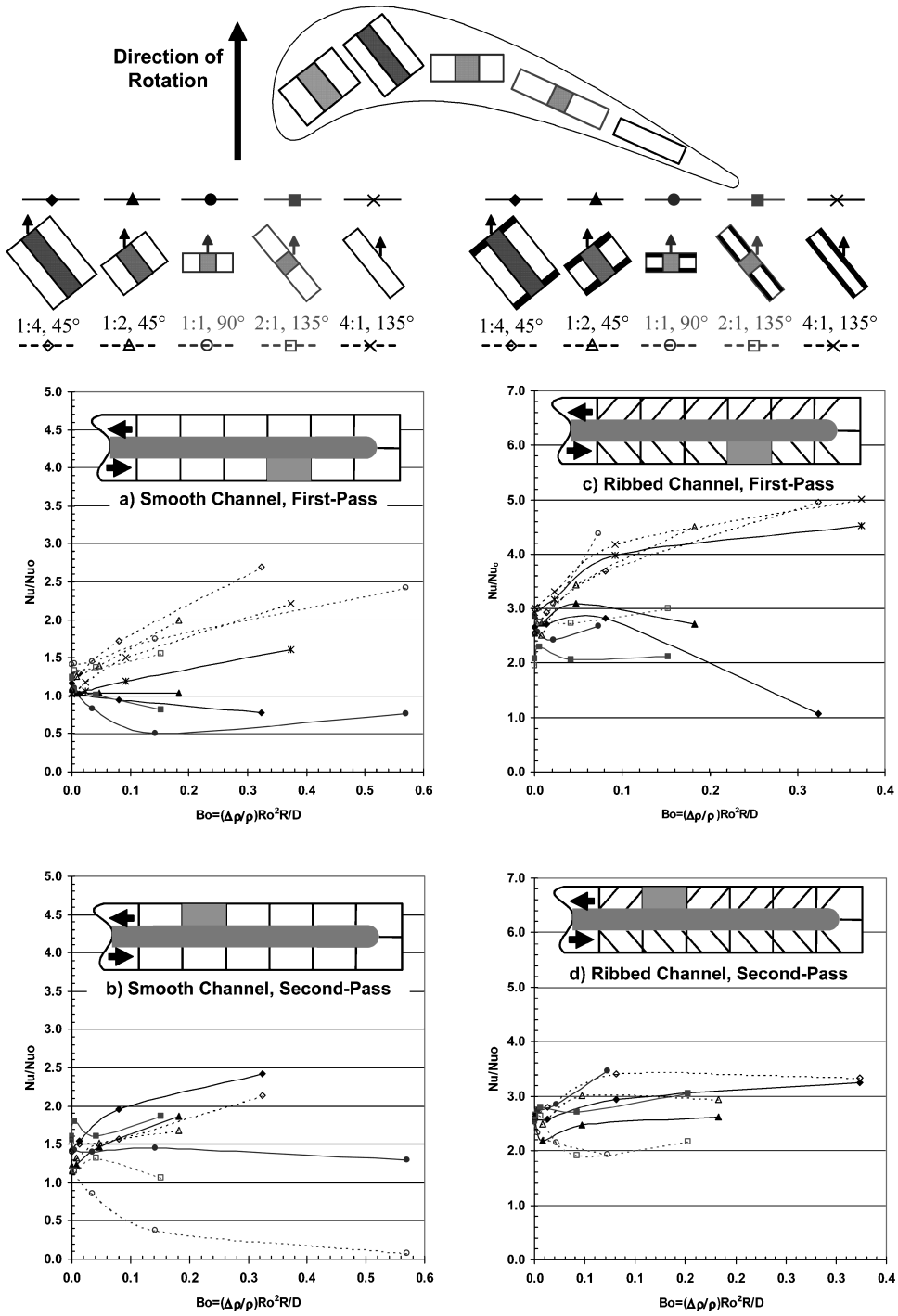

Fig. 6 Heat transfer enhancement in rotating smooth and ribbedchannels.

with various aspect ratios and orientation angles; channels with aspect ratios of 1:4 (Refs. 46 and 47), 1:2 (Refs. 46 and 47), 1:1 (Refs. 26 and 27), 2:1 (Ref. 35), and 4:1 (Ref. 37) are considered. The heat transfer enhancement is shown for one region in the first pass and one region in the second pass; these regions are sufficiently far from the entrance (first pass) and the turn (second pass) to represent fully developed flow for each pass. Because the orientation of the cooling passage varies to fit the cross section of a given blade, the various aspect ratio channels are shown at various orientations depending on the probable location in a turbine blade. For all aspect ratios with smooth walls, the heat transfer enhancement on the trailing surfaces in the first pass is increasing with the increasing buoyancy parameter. However, the heat transfer decreases on the leading surface of the 2:1 and 1:4 channels, whereas it increases on the leading surfaces of the 4:1 channel. Furthermore, for the 1:1 channel, the leading surface heat transfer decreases then increases at higher buoyancy parameter. In the second pass of channels with smooth walls, both the leading and trailing surfaces of the 1:4 and 1:2 channels undergo heat transfer enhancement with the increasing buoyancy parameter, and the trailing surfaces of the 1:1 and 2:1 channels experience a decrease, whereas the leading surfaces see an enhancement in the Nusselt number ratios. The trends for the heat transfer enhancement in channels with angled ribs are less discernable due to the variation in rib geometry. The same size ribs were used in each channel; therefore, the rib height-to-hydraulic diameter (or rib height-to-channel height) ratio varies between the channels.

Heat Transfer in Rotating Coolant Passages with Trapezoidal Cross-Section

In the literature, most internal coolant passage geometries are idealized as square, triangular, or rectangular cross-sectional channels. Rathjen et al.[48] studied detailed heat/mass transfer distributions in a

rotating two-pass coolant channel with engine near cross section and smooth walls. The test section consisted of a first pass with trapezoidal cross section for radial outward flow, a 180-deg bend with a 90-deg turning vane, and a second pass with a larger trapezoidal cross section for radial inward flow. Note that the channel cross section and orientation in this study are for the midchord to leading edge of real rotor coolant passage geometry. They used the naphthalene sublimation technique to obtain detailed heat/mass transfer distributions and CFD for complex flowfield simulations. They found that the heat/mass transfer distributions in the bend and in the region after the bend show strong gradients with several separation zones and that the flow is forced to follow the turbine blade shape, that is, channel shape and orientation with respect to the axis of rotation.

Fluid Flow in Rotating Coolant Passages

Heat transfer is a side effect of the flowfield. Flow in a rotating channel is significantly different from flow in a nonrotating channel. The secondary flow in rotation redistributes velocity and also alters the random velocity fluctuation patterns in turbulent flows. Lezius and Johnston[49] examined flow instability caused by rotation in a straight rectangular channel with smooth walls. They reported that rotation increases flow velocity and turbulence near the unstable trailing wall and reduces the turbulent fluctuations significantly near the stable leading wall. Elfert[50] measured velocity and turbulence distributions in a rotating circular pipe. Rotation shifts the bulk flow toward the trailing side, and the turbulence profile shows a different distribution in rotation. Tse and McGrath[51] used laser Doppler velocimetry to measure rotating flow in a two-pass channel with smooth and ribbed walls. Tse and Steuber[52] investigated the mean flow characteristics in the first and second passages of a rotating four-pass coolant passage with 45-deg ribs of semicircular cross section using laser Doppler anemometry (LDA). Cheah et al.[53] used LDA to measure velocity and turbulence quantity in a rotating two-pass channel. Bons and Kerrebrock[54] measured the internal flow in a straight smooth-wall channel with particle image velocimetry (PIV) for both heated and nonheated cases. Schabacker et al.[55] and Chanteloup et al.[56] also used PIV to measure the flows in stationary two-pass square ducts with 45-deg turbulators. Son et al.[57] measured the flows in two-pass channels with smooth and 90-deg ribbed walls using PIV. Liou and Chen[58] measured the developing flow in a two-pass channel with LDA. Liou et al.[59] studied fluid flow in a rotating two-pass duct with in-line 90-deg ribs using LDA. Liou et al.[60] also performed LDV and pressure measurements for in-line detached 90-deg ribs. Liou and Dai[61] measured pressure and flow characteristics in a rotating two-pass square duct with 45-deg angled ribs of square cross section by using LDA. The 45-deg ribs are found to reduce the pressure loss by 60% in comparison with the 90-deg ribs. Liou et al.[62] measured flow and pressure fields in a rotating two-pass duct with staggered 45-deg ribs of rounded cross section. They found that the staggered 45-deg ribs reduce the friction loss to $88\% \pm 1\%$ of that of the in-line 45-deg ribs. Both Liou and Dai[61] and Liou et al.[62] reported that the absence of a periodic fully developed flow condition in their tests. The mentioned flow measurements help to understand the flow physics and serve to explain the heat transfer results obtained in two-pass rotating channels with smooth and ribbed walls.

Computational Heat Transfer in Rotating Coolant Passages

In recent years, several researchers have made computational studies on internal cooling channels of the rotating blade. Numerical predictions provide the details that are difficult to obtain by experiments. Moreover, the increase in computation power in desktop computers has made it economical to optimize the design parameters based on numerical analyses. Most common models are based on a two-equation turbulence model, namely, the k–ε model, low Reynolds number k–ε model, the two-layer k–ε model, and the low Reynolds number k–ω model. The advanced Reynolds stress model and the second-moment closure model are also employed. In general, it has been proven by many investigators that the k–ε model cannot correctly predict the complex flow and heat transfer behaviors in rotating two-pass rectangular channels with angled rib-type turbulence promoters typically in the rotor coolant passage design. This is simply due to the isotropic turbulence assumption and near-surface wall function requirement made by using the k–ε model. However, there are much more complicated flowfields in the rotor coolant passage design such as rotating three-dimensional asymmetric flow, 180-deg turning and recirculation, angled rib-induced flow separation and secondary flow, etc. It has been found by previous investigators that the low Reynolds number k–ω model does predict reasonably well the flow and heat transfer in typical two-pass rotating channels with angled ribbed walls. This is attributed to the fact that the turbulence dissipation is specified in terms of the turbulent kinetic energy in the near-wall region to replace wall function and that very fine grid computation is used toward the surface. As expected, the second-moment closure model provides the best flow and heat transfer characteristics in typical rotating two-pass channels with angled rib turbulators. In this model, six additional transport equations are required to be solved in a three-dimensional turbulent flow, and the eddy diffusivity in the momentum transport equation is replaced by the source terms developed from the turbulent Reynolds stress tensor. Therefore, more computing time is required. In the following paragraphs, only a few representative studies using the low Reynolds number k–ω model and second-moment closure model are mentioned.

Dutta et al.[63] used a rotation-modified k–ε turbulence model to predict heat transfer coefficients in different aspect ratio rotating straight channels (aspect ratios equal to 1:4–4:1) with smooth walls. They found that rotation has more effect on lower aspect ratio channel (1:4) than high aspect ratio channel (4:1). Stephens et al.[64] predicted the flow and heat transfer in a rotating two passage square duct with smooth walls using a low Reynolds number k–ω model. Lin et al.[65] used the same low Reynolds number k–ω model in their investigation of the effect of 45-deg angled ribs on the heat transfer coefficients in a rotating two-pass square channel. They studied the effects of compressible-flow Reynolds numbers, rotation numbers, and buoyancy parameters. They found that the angled ribs create an asymmetric heat transfer coefficient distribution. This is because the angled ribs developed a secondary flow of their own and that interacts with the secondary flow developed in rotation. In the leading wall of the radial outward flow, heat transfer is highest at the upstream side of the rib and in the interrib region next to the inner sidewall. However, for the radial inward flow after the 180-deg bend, heat transfer is highest on the upstream side of the rib and in the interrib region next to the outer sidewall. They did not compare with the experimental data. Bonhoff et al.[66] calculated the heat transfer coefficients and flowfields for rotating U-shaped square channels with 45-deg angled ribs by using a Reynolds stress turbulence model (RSM) with wall functions in the FLUENT CFD code. Their results show that the heat transfer coefficients of the rotating first-pass leading and trailing surfaces are underpredicted by the experimental data. Sleiti and Kapat[67] also used the FLUENT code to calculate the flow and heat transfer in rotating two-pass ribbed channels under high rotation number and high density ratio conditions. Their RSM results are better than those obtained by Bonhoff et al.[65] due to the use of enhanced near-wall treatment and tuned coefficients. Iacovides and Raisee[68] explored turbulence modeling issues related to the computation of flow and heat transfer in internal cooling passages of turbine blades with 90-deg ribs. They found that the low Reynolds differential stress model reproduces the turbulence field more reasonably than the k–ε model. Jang et al.[69] predicted flow and heat transfer in a single-pass rotating square channel with 45-deg angled ribs by the second-moment closure model. Their heat transfer coefficient prediction compared well with the experimental data. This has affirmed the superiority of the second-moment closure model compared to the simpler isotropic eddy viscosity k–ε model. The advantage of the second-moment closure model is that it resolves the near-wall flow all of the way to the solid wall rather than using the log-law assumption in the viscous sublayer. With this near-wall closure, surface data such as heat transfer coefficients and friction factors can be evaluated directly from velocity and temperature gradient on the solid wall. Al-Qahtani et al.[70] predicted flow and heat transfer in a two-pass rotating rectangular channel (aspect ratio $AR = 2{:}1$) with 45-deg

angled ribs by the same second-moment closure model used by Jang et al.[69] They[70] found that the predicted heat transfer coefficient compared reasonably well with the experimental data of Azad et al.[35]

Al-Qahtani et al.[71] also conducted a numerical study of flow and heat transfer in one-pass rotating rectangular channels (AR = 4:1) with 45-deg rib turbulators using the same second-moment closure model. Their heat transfer predictions were in good agreement with the experimental data of Griffith et al.[37] Jia et al.[72] predict local heat transfer and fluid flow behaviors in stationary straight square duct with transverse and V-shaped ribs by using a RSM. They concluded that V-shaped ribs pointing upstream had superior performance compared to V-shaped ribs pointing downstream and transverse ribs. Using the same second-moment closure model as Jang et al.,[69] Su et al.[73] computed flow and heat transfer in one-pass rotating rectangular channels (AR = 4:1) with V-shaped rib turbulators for a wide range of Reynolds numbers from 1×10^4 to 5×10^5. Their heat transfer predictions were in good agreement with the experimental data of Lee et al.[39] Results show that the V-shaped ribs induce four counter-rotating vortices that vary in size along the streamwise direction. However, the rotation-induced cross-stream secondary flow distorts the V-shaped rib-induced vortices and affects the heat transfer on both leading and trailing surfaces with V-shaped ribs. Results also show that the V-shaped ribs create a symmetric heat transfer enhancement from the channel centerline toward the sidewalls, the rotation increases heat transfer enhancement on the trailing surface and decreases heat transfer enhancement on the leading surface, and higher Reynolds numbers tend to weaken the heat transfer enhancement effect of the V-shaped rib-induced secondary flow. Su et al.[74,75] also studied the flow and heat transfer in rotating two-pass square (AR = 1:1) and low aspect ratio (AR = 1:2 and 1:4) rectangular channels with smooth walls and 45-deg angled ribs. A total of 30 test cases were investigated with various combinations of Reynolds numbers ($Re = 1 \times 10^4$ and 1×10^5), rotation numbers (0.0, 0.14, and 0.28), and coolant-to-wall density ratios (0.13, 0.20, and 0.40). For the low Reynolds number and low rotation number cases, they found that the rotation effect on the Nusselt number and friction factor ratios is more significant in the AR = 1:2 channel than those observed in either the square or AR = 1:4 channel due to the presence of strong turn-induced vortices. For the high rotation number and high Reynolds number cases, however, the rotation effect decreases continuously when the channel aspect ratio was changed from AR = 1:1 to 1:2 and 1:4.

The cited numerical investigations demonstrated that the advanced second-order RSMs (second-moment) are capable of providing detailed three-dimensional velocity, pressure, temperature, Reynolds stresses, and turbulent heat fluxes that were not previously available in most of the experimental studies. In this paper, we will systematically examine some of the second-moment results for various turbine blade cooling passages to facilitate a detailed investigation of the effects of blade rotation, rib geometry, channel aspect ratio, and channel orientation on the turbulent flow productions and the associated heat transfer enhancements. For brevity, however, we will present only the numerical results obtained by the authors' research group using the near-wall second-moment closure of Chen et al.[76,77] For other second-order Reynolds stress closure models refer to recent papers mentioned earlier.

Governing Equations

All of the numerical results presented here were obtained using the near-wall second-order Reynolds stress closure model of Chen et al.[76,77] The method solves the nondimensional RANS equations in general curvilinear coordinates (ζ, t):

$$\frac{\partial \rho}{\partial t} + (\rho U^m)_{,m} = 0 \tag{1}$$

$$\rho\left(\frac{\partial U^i}{\partial t} + U^m U^i_{,m} + R^{im}_{,m}\right) + 2\rho g^{il} e_{lmn} \mathbf{\Omega}^m U^n + \rho g_{mn}(\mathbf{\Omega}^i \mathbf{\Omega}^m \xi^n - \mathbf{\Omega}^m \mathbf{\Omega}^n \xi^i) = -g^{im} p_{,m} + \left(\mu g^{mn} U^i_{,n}\right)_{,m} \tag{2}$$

where e_{lmn} is the third-rank permutation tensor and $\mathbf{\Omega}^m$. is the rotation vector. The metric tensor g_{mn} and conjugate metric tensor g^{mn} are given by Chen et al.[78] $R^{im} = \overline{u^i u^m}$ is the Reynolds stress tensor. Overbars denote that the ensemble Reynolds averaging and the summation convention are used for repeated indices. The subscript $,m$ represents the covariant derivative with respect to ξ^m. U^i and u^i are contravariant components of the mean and fluctuating velocities, t is time, and p is pressure. In Eq. (2), $2\rho g^{il} e_{lmn} \mathbf{\Omega}^m U^n$ is the Coriolis force and $\rho g_{mn}(\mathbf{\Omega}^i \mathbf{\Omega}^m \xi^n - \mathbf{\Omega}^m \mathbf{\Omega}^n \xi^l)$ is the centrifugal force. In the present study, the flow is considered incompressible because the Mach number is quite low. However, the density in the centrifugal force terms is approximated by $\rho = \rho_0 T_0 / T$ to account for the density variations caused by the temperature differences. Here ρ_0 and T_0 are the density and temperature at the inlet of the cooling channel. The density variation in the centrifugal force terms produces centrifugal buoyancy effects and accounts for different centrifugal accelerations between the cooler (heavier) and hotter (lighter) fluids at the same radial distance from the center of rotation. Note that the magnitude of centrifugal buoyancy force is inversely proportional to the fluid temperature. The net effects of the centrifugal buoyancy force tend to slow down the hotter fluid more than the cooler fluid and distort the velocity profiles by moving the high-momentum fluid toward the cooler surface.

The temperature T is obtained from the energy equation:

$$\rho c_p\left[\frac{\partial T}{\partial t} + U^m T_{,m} + (\overline{u^m T'})_{,m}\right] = g^{mn}(K T_{,n})_{,m} + \frac{\mathrm{D}p}{\mathrm{D}t} + \Phi \tag{3}$$

$$\Phi = \mu\left[U^m_{,n} U^n_{,m} + \overline{u^m_{,n} u^n_{,m}} + g_{ij} g^{mn}\left(U^i_{,m} U^j_{,n} + \overline{U^i_{,m} u^j_{,n}}\right)\right] \tag{4}$$

where T and T' are the mean and fluctuating temperature fields, Φ is the dissipation function, C_P is the specific heat at constant pressure, K is the thermal conductivity, and $\overline{u^m T'}$ is the kinematic turbulent heat flux.

The Reynolds stress tensor $R^{ij} = \overline{u^i u^j}$ is the solution of the transport equations

$$\frac{\partial R^{ij}}{\partial t} + U^m R^{ij}_{,m} = P^{ij} + D^{ij}_u + D^{ij}_p + D^{ij}_v + \Phi^{ij} - \varepsilon^{ij} \tag{5}$$

Each term is defined as follows.

Production:

$$P^{ij} = -\left(R^{im} U^j_{,m} + R^{jm} U^i_{,m}\right) - 2e_{lmn}\Omega^m (g^{il} R^{jn} + g^{jl} R^{in})$$

Diffusion by u^m:

$$D^{ij}_u = -(\overline{u^i u^j u^m})_{,m}$$

Diffusion by p':

$$D^{ij}_p = -g^{jm}(\overline{u^i p'/\rho})_{,m} - g^{im}(\overline{u^j p'/\rho})_{,m}$$

Viscous diffusion:

$$D^{ij}_v = \nu g^{mn} R^{ij}_{,mn}$$

Pressure–strain:

$$\Phi^{ij} = \overline{(p'/\rho)\left(g^{im} u^j_{,m} + g^{jm} u^i_{,m}\right)}$$

Dissipation:

$$\varepsilon^{ij} = 2\nu g^{mn} \overline{u^i_{,m} u^j_{,n}}$$

To solve these equations, appropriate closure models must be provided for the pressure–strain, diffusion, and dissipation terms. In the present study, the combined diffusion terms are models by the gradient model of Daly and Harlow,[79]

$$D^{ij} = D^{ij}_u + D^{ij}_p = C'_s\left[(k/\varepsilon) R^{mn} D^{ij}_{,n}\right]_{,m}, \qquad C'_s = 0.22 \tag{6}$$

The pressure–strain and the dissipation terms were modeled together using the pressure–strain correlation of Speziale et al.[80] and the near-wall Reynolds stress closure of Chen,[81,82]

$$\Phi^{ij} - \varepsilon^{ij} = \bar{\Phi}^{ij}_1 + \Phi^{ij}_2 + \Phi^{ij}_w - \tfrac{2}{3} g^{ij} \varepsilon \tag{7}$$

Where

$$\bar{\Phi}^{ij}_1 = -\bar{C}_1\{1 - (1/\bar{C}_1) f_w\}\varepsilon b^{ij} + C_2(1 - f_w)\varepsilon\left(g_{mn} b^{im} b^{jn} - \tfrac{1}{3} g^{ij} II\right) \tag{8}$$

$$\Phi_2^{ij} = \left(C_3 - C_3^* II^{\frac{1}{2}}\right)kS^{ij} + C_4k\left(g_{mn}b^{im}S^{jn} + g_{mn}b^{jm}S^{in} - \tfrac{2}{3}g^{ij}II\right) + C_5k\left(g_{mn}b^{im}W^{jn} + g_{mn}b^{jm}W^{in}\right) \quad (9)$$

$$\Phi_w^{ij} = f_w\left\{0.45\left(p^{ij} - \tfrac{2}{3}g^{ij}P\right) - 0.03\left(Q^{ij} - \tfrac{2}{3}g^{ij}P\right) + 0.08k(2S^{ij})\right\} \quad (10)$$

$$b^{ij} = R^{ij}/2k - \tfrac{1}{3}g^{ij}, \qquad II = g_{mr}g_{ns}b^{mn}b^{rs} \quad (11)$$

$$S^{ij} = \tfrac{1}{2}\left(g^{jm}U^i_{,m} + g^{im}U^j_{,m}\right), \qquad W^{ij} = \tfrac{1}{2}\left(g^{jm}U^i_{,m} - g^{im}U^j_{,m}\right) \quad (12)$$

$$P = \tfrac{1}{2}g_{mn}P^{mn}, \qquad Q^{ij} = -g_{lm}(g^{in}R^{jl} + g^{jn}R^{il})U^m_{,n} \quad (13)$$

$$\bar{C}_1 = C_1 + C_1^*(P/\varepsilon), \qquad f_w = \exp\left[-\left(0.0184Re\sqrt{k}y\right)^4\right] \quad (14)$$

where the model coefficients C_1, C_1^*, C_2, C_3, C_3^*, C_4, and C_5 are equal to 3.4, 1.80, 4.2, 0.8, 1.30, 1.25, and 0.40, respectively.

In the present model, the turbulent heat fluxes $\overline{u^mT'}$ are modeled using the generalized gradient diffusion hypothesis given by Bo et al.,[83]

$$\overline{u^mT'} = -C_\theta(k/\varepsilon)R^{mn}T_{,n}, \qquad C_\theta = 0.0225 \quad (15)$$

Note that the C_θ value used here is somewhat lower than that proposed by Bo et al.[83] based on extensive numerical optimizations performed in the present calculations.

Cooling Channel Configurations

In this paper, we shall focus on the predicted secondary flow patterns for a wide range of cooling channel configurations to facilitate a detailed understanding of the turbulent flow characteristics induced by the channel bend curvature, turbine blade rotation, coolant-to-wall density ratio channel aspect ratio, and channel orientation. In general, the secondary flow in the rectangular cooling channels may be induced by several different mechanisms including 1) Reynolds stress anisotropy, 2) 180-deg turn, 3) ribbed turbulators, 4) channel rotation, and 5) temperature difference. These secondary flows will be discussed in the following sections for different aspect ratio ducts.

To facilitate the discussion of the numerical simulation results, we will define the most important geometric and flow parameters for cooling channels using the AR = 2:1 rectangular channel as an example. Figure 7 shows the geometry of the AR = 2:1 two-pass rectangular channel with 45-deg angled ribs that was investigated experimentally by Azad et al.[35] and numerically by Al-Qahtani et al.[70] Here, the aspect ratio is defined as the ratio of the channel width (ribbed walls, leading and trailing surfaces) to the channel height (smooth walls). Calculations were also performed by Al-Qahtani et al.[84] for the same channel configuration with smooth walls. The hydraulic diameter D_h of this AR = 2:1 channel is 0.667 in. (1.69 cm), and the radius of curvature of the 180-deg sharp turn is $r_i/D_h = 0.375$. In the ribbed section, the leading and trailing surfaces for both the first and second passages are roughened with nine equally spaced ribs of square cross section. The rib height-to-hydraulic diameter ratio (e/D_h) is 0.094, and the rib-pitch-to-height ratio (P/e) is 10. All ribs are inclined at an angle $\alpha = 45$ deg with respect to the flow. Two channel orientations were studied: $\beta = 90$ deg corresponding to the midportion of a turbine blade and $\beta = 135$ deg corresponding to the serpentine passages in the trailing edge region of a blade.

Al-Qahtani et al.[71] also investigated the flow and heat transfer in another higher aspect ratio (AR = 4:1) one-pass rectangular channel with smooth walls and 45-deg angled ribs. More recently, Su et al.[74,75] performed parametric studies of fluid flow and heat transfer characteristics for the square and low aspect ratio rectangular channels with smooth walls and 45-deg angled ribs. A total of 30 test cases were performed for AR = 1:1, 1:2, and 1:4 rectangular channels including high Reynolds number, high rotation number, and high coolant-to-wall density ratio conditions. These cooling channels have the same length, same bend radius (except for the AR = 4:1 case, which has only one passage), and the same rib arrangements (45-deg in-line ribs with the same rib height and pitch) as that shown in Fig. 7. Note, however, that the hydraulic diameter varies with the aspect ratio in the experiments of Azad et al.[35] and Fu et al.[46,47] for different aspect ratio ducts because the narrow sides of the rectangular channels are kept at 0.5 in (1.27 cm) in all experimental investigations. For the low aspect ratio channels, the channel width remains the same, but the channel height was increased from 0.5 in. (1.27 cm) to 1.0 (2.54) and 2.0 in. (5.08 cm) for AR = 1:2 and 1:4 channels. For AR = 1:2 and 1:4 channels, the ribs were placed on the narrow sides so that the rib geometrties for these channels are identical to those installed in the square channel. On the other hand, the height of high aspect ratio channels remains the same at 0.5 in. (1.27 cm) and the channel width was increased to 1.0 (2.54) and 2.0 in. (5.08 cm) for the AR = 2:1 and 4:1 ducts, respectively. For high aspect ratio channels, the ribs were placed on the broad side of the channels so that the rib length increases with increasing channel aspect ratio. Note that the square channel has the smallest hydraulic diameter of 0.5 in. (1.27 cm), whereas the AR = 1:4 and 4:1 channels have the largest hydraulic diameter of 0.8 in. (2.03 cm). Therefore, at the same Reynolds number, the square channel has the highest channel inlet velocity and the highest e/D_h ratio. These must be borne in mind when comparing the fluid flow and heat transfer characteristics for different aspect ratio ducts. In this paper, we will compare the results for all five different aspect ratio ducts (AR = 4:1, 2:1, 1:1, 1:2, and 1:4) to facilitate a detailed understanding of the three-dimensional flow and heat transfer in rotating cooling channels.

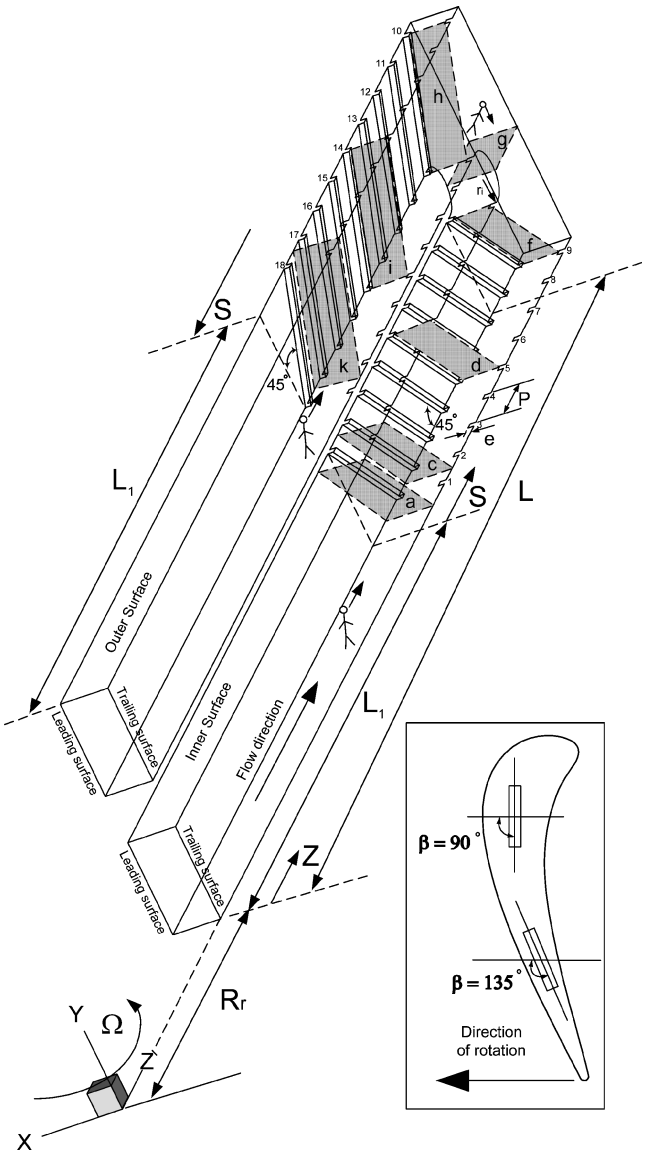

Fig. 7 Geometry for two-pass AR = 2:1 rectangular channel with 45-deg ribs (A1-Qahtani et al.[70]): $R_r/D_h = 20.0$, $L/D_h = 20.34$, $r_i/D_h = 0.375$, $L_r/D_h = 12.84$, $e/D_h = 0.094$, and $P/e = 10$.

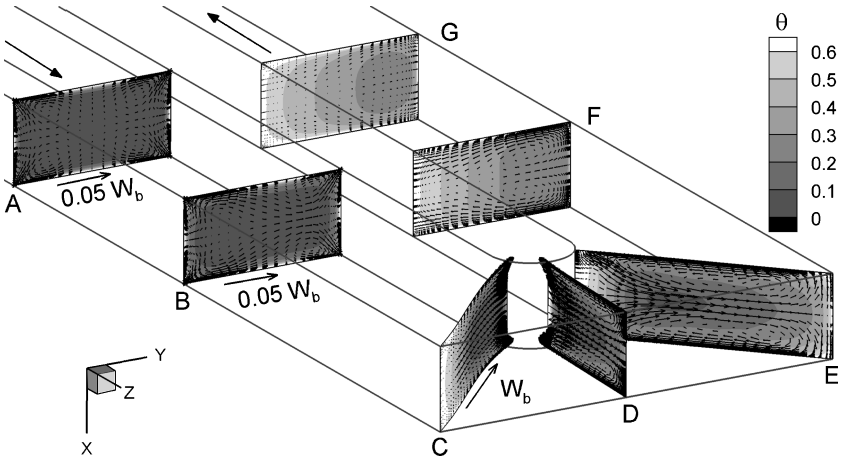

Fig. 8 Temperature contours and secondary flows in nonrotating AR = 2:1 rectangular duct ($Re = 10^4$).

Reynolds Stress-Driven Secondary Flow

Most of the cooling channels in practical turbine blade designs involve serpentine channels with several 180-deg turns. These bends force the mainstream flow to turn in opposite directions between radially inward and radially outward flow conditions. Figure 8 shows the secondary flow pattern and temperature contours at seven selected cross sections around the bend region for the nonrotating $AR = 2{:}1$ smooth channel at $Re = 1 \times 10^4$ as tested by Al-Qahtani et al.[84] It is seen that the secondary flow pattern is rather complex even for the relatively simple non-rotating smooth duct without additional complications due to the rib turbulators and/or channel rotation. In this section, we shall examine first the Reynolds stress-induced secondary flow in the first passage before the 180 turn. The bend-induced secondary flow will be discussed in the next section.

In the first passage before the turn (stations A and B, Fig. 8),there are four pairs of counter-rotating vortices in the corner region of the straight channel. Note that these vortices are significantly weaker than the bend-induced vortices as the velocity scale for stations A and B is only 1/20th of that for the other five stations C–G in the bend region and the second passage. It is well known that these corner vortices are induced by the Reynolds stress anisotropy in the near-wall region. The Reynolds stress component normal to the surface is directly impeded by the wall and is the smallest among the three normal stress components. On the other hand, the Reynolds stress in the streamwise direction is the largest because it is unimpeded by the wall and also enhanced by the streamwise velocity gradient. Chen et al.[77] presented detailed Reynolds stresses and turbulent heat fluxes in the first passage, the midsection of the bend, and the second passage of a nonrotating smooth square duct. Both the Reynolds stresses and turbulent heat fluxes exhibit a high degree of anisotropy. In the present near-wall second-moment closure, the pressure–strain terms are linearly proportional to the anisotropic tensor b^{ij} [Eq. (8)], which measures the degree of anisotropy in normal stress components. Furthermore, each production term in the Reynolds stress model responds differently to different components of the mean rates of strain in a complex three-dimensional flowfield. Because each Reynolds stress component is calculated directly using its respective transport equation, it enables us to predict accurately the highly anisotropic Reynolds stress components in the wall boundary layer and the turbulence-driven corner vortices.

Figure 9 shows a comparison of the secondary flow patterns for five different aspect ratio channels in the first passage before the turn at $Re = 1 \times 10^4$. For the square duct, the anisotropy of the turbulent Reynolds stresses produced eight small secondary corner vortices, which are symmetric with respect to the duct center planes. These vortices grow along the broad side as the channel aspect ratio changes from $AR = 1{:}1$ to $AR = 1{:}2$ or 2:1. However, the vortices cease 19 to expand when the channel aspect ratio was further changed to $AR = 1{:}4$ or 4:1. Note that these turbulence-driven vortices can only be predicted by nonisotropic turbulence models such as the Reynolds stress or algebraic stress models.

Bend-Induced Secondary Flow

As noted earlier in Fig. 8, the Reynolds stress-driven secondary flows before the turn are significantly weaker than the pressure-driven secondary flow in the 180-deg turn and downstream of the bend. As the fluid flows through the 180-deg bend, the centrifugal forces arising from the curvature and the associated pressure gradients (low pressure at inner surface, high pressure at outer surface) produced a pair of symmetric, counter-rotating vortices in the bend. These vortices are responsible for the transport of cool fluid from the core toward the outer surface. Before the bend, the cooler fluid is located in the core region. After the bend, however, the cooler fluid is pushed toward the outer surface by the centrifugal force induced by the streamline curvatures. This leads to steeper temperature gradients and higher heat transfer on the outer wall than on the inner wall after the bend.

The strength of the secondary flows in the bend region depends on the bend geometry, as well as the aspect ratio of the duct. For large turning radius (compared to the hydraulic diameter of the duct), the flow remain attached downstream of the bend. However, separation regions were often observed behind sharp bends. Figure 10 shows the secondary flow patterns and temperature contours in the turn regions of four different aspect ratio smooth ducts as tested by Al-Qahtani et al.[84] and Su et al.[74] Note that there are no experimental or numerical results for the $AR = 4{:}1$ case because it has only one single passage (without the 180-deg bend) and is used exclusively in the trailing-edge section, where the blade thickness is small. Note in Fig. 10 that there are distinct differences in the secondary flow patterns for different aspect ratio ducts. For the square ($AR = 1{:}1$) and $AR = 2{:}1$ ducts, the counter-rotating vortex pair generated by the bend is squashed in the vertical direction due to the tight spacing between the leading and trailing surfaces. In the low aspect ratio rectangular ducts, however, the vortices induced by the 180-deg turn tend to maintain circular shapes up to the space limitations rather than expanding continuous in the vertical direction. In the $AR = 1{:}1$ and 1:2 channels, the counter-rotating vortices occupy the entire channel and bring cooler fluid in the core region toward the outer surface. For the $AR = 1{:}4$ channel, however, the nearly circular vortex pair is confined to the leading and trailing surfaces. Even though the secondary flow is very weak in the middle section of the $AR = 1{:}4$ channel, the additional pressure gradients induced by the counter-rotating vortices still apply over the entire channel cross section. Consequently, the cooler fluid in the middle section of the $AR = 1{:}4$ channel was pushed by the vortex-induced pressure gradients back toward the inner surface as seen in the corresponding temperature contours shown in Fig. 10.

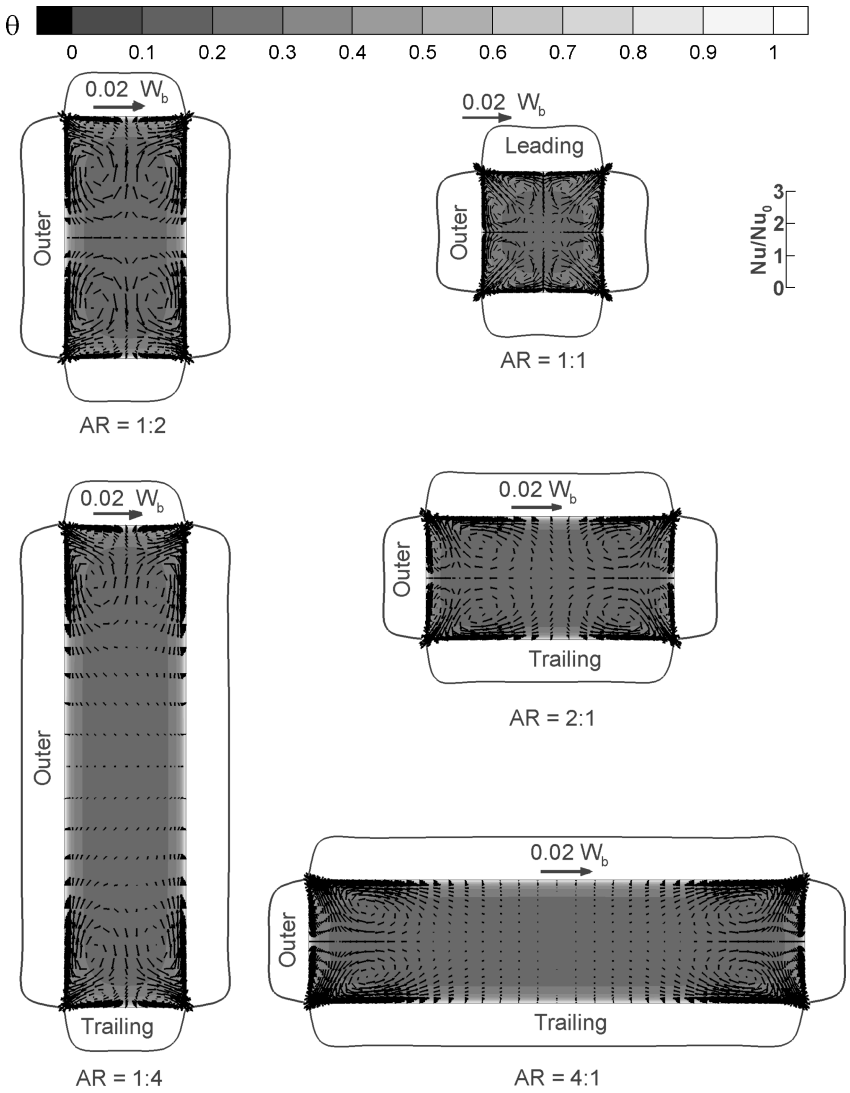

Fig. 9 Temperature contours and turbulence-induced secondary flows in the first passage (before 180-deg turn) of nonrotating rectangular ducts ($Re = 10^4$).

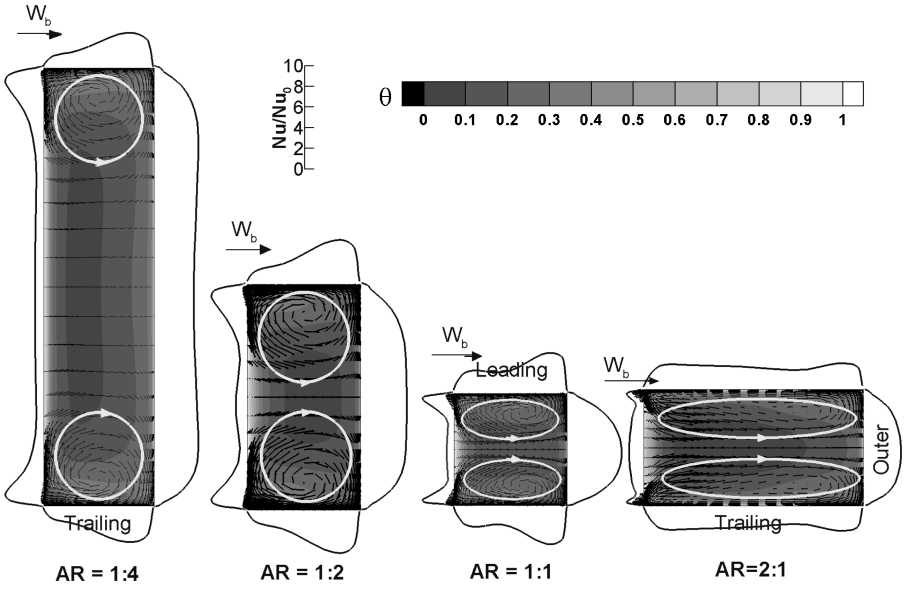

Fig. 10 Temperature contours and secondary flows in midsection of the bend of nonrotating rectangular ducts ($Re = 10^4$).

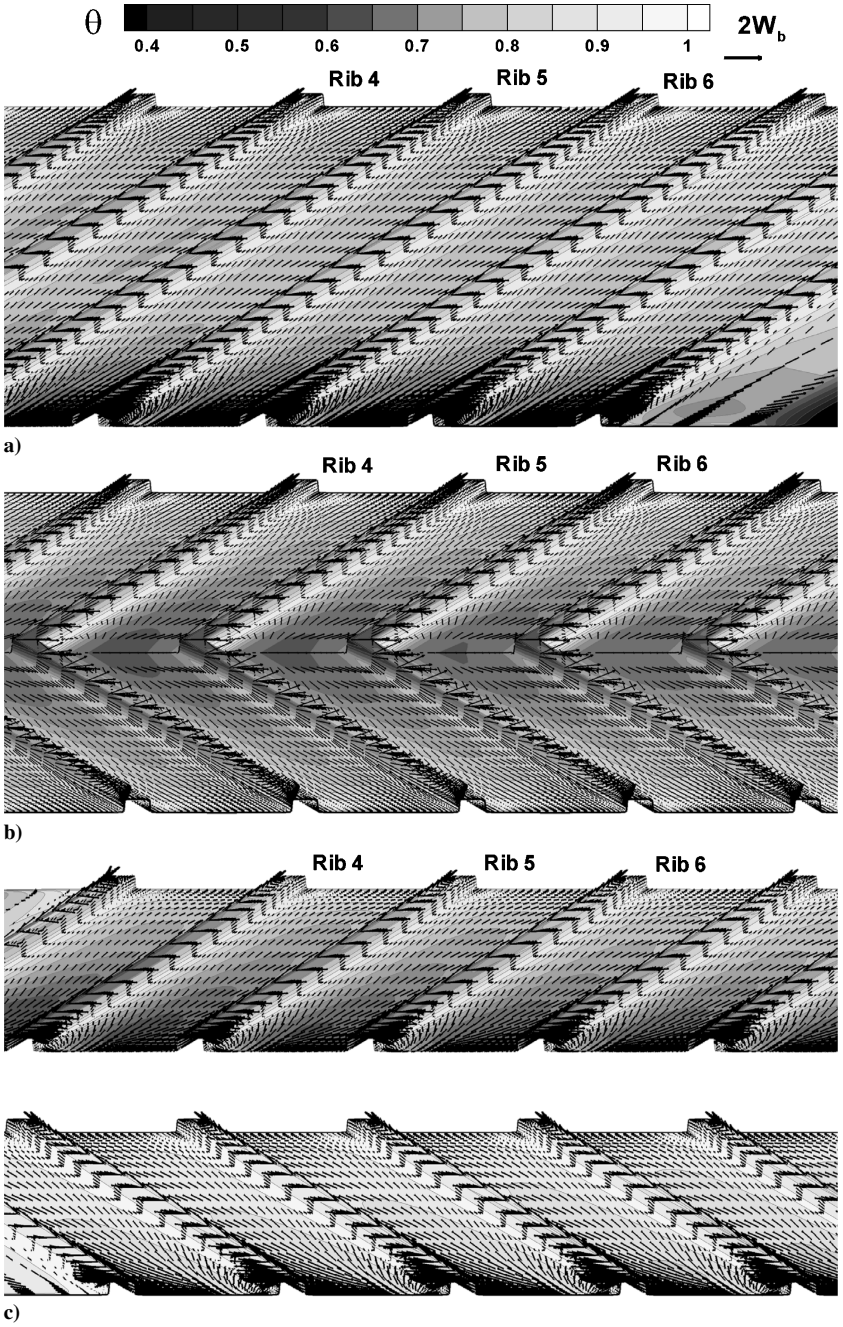

Fig. 11 Velocity vectors and temperature contours: a) AR = 4:1 one-pass channel with 45-deg inclined ribs, b) AR = 4:1 one pass channel with V-shaped ribs, and c) AR = 2:1 two-pass channel with 45-deg inclined ribs ($Re = 1 \times 10^4$).

Rib-Induced Secondary Flow

As noted earlier, advanced gas turbines often use rib turbulators on two opposite walls of internal cooling passages to augment heat transfer. Many different rib configurations have been investigated experimentally over the past decade with various combinations of rib height, rib angle, rib spacing, rib shape, and in-line or staggered rib arrangements. In this section, we examine the rib-induced secondary flow for the 45-deg in-line angled ribs and V-shaped ribs in square and rectangular channels as reported by Al-Qahtani et al.[71,84] and Su et al.[73,74] The effects of rib angle and rib shape will be discussed in later sections.

Figure 11a shows the secondary flow induced by the 45-deg inclined ribs in a one-pass AR = 4:1 nonrotating channel, which was investigated by Al-Qahtani et al.[71] The angled ribs induced secondary flow that moves parallel to the ribs from the inner (bottom) to outer (top) surface. Because the ribs are oriented at a 45-deg angle, the fluid adjacent to the bottom (inner) surface will reach the ribs first and move along the ribbed surface toward the top (outer) surface. It then returns back to the bottom surface along the centerline of the inclined cross-stream plane as seen in Fig. 12a. In Fig. 12a, one can clearly see that the ribs induced two symmetric counter-rotating vortices that impinge on the inner (bottom) surface. The temperature contour is closely related to the streamwise flow separation and reattachment as well as the secondary flow patterns induced by the inclined ribs. The temperature is high immediately downstream of each rib due to flow separation behind the ribs. In the middle section between the ribs, however, the temperature is relatively low due to the impingement of cooler fluids in the flow reattachment zone. Also, the temperature increases gradually from the inner toward the outer surface as the cooler fluid is convected along the ribbed surface toward the outer (top) surface.

Figure 11b shows the velocity vector field and dimensionless temperature contours near the ribbed surface for a 4:1 nonrotating

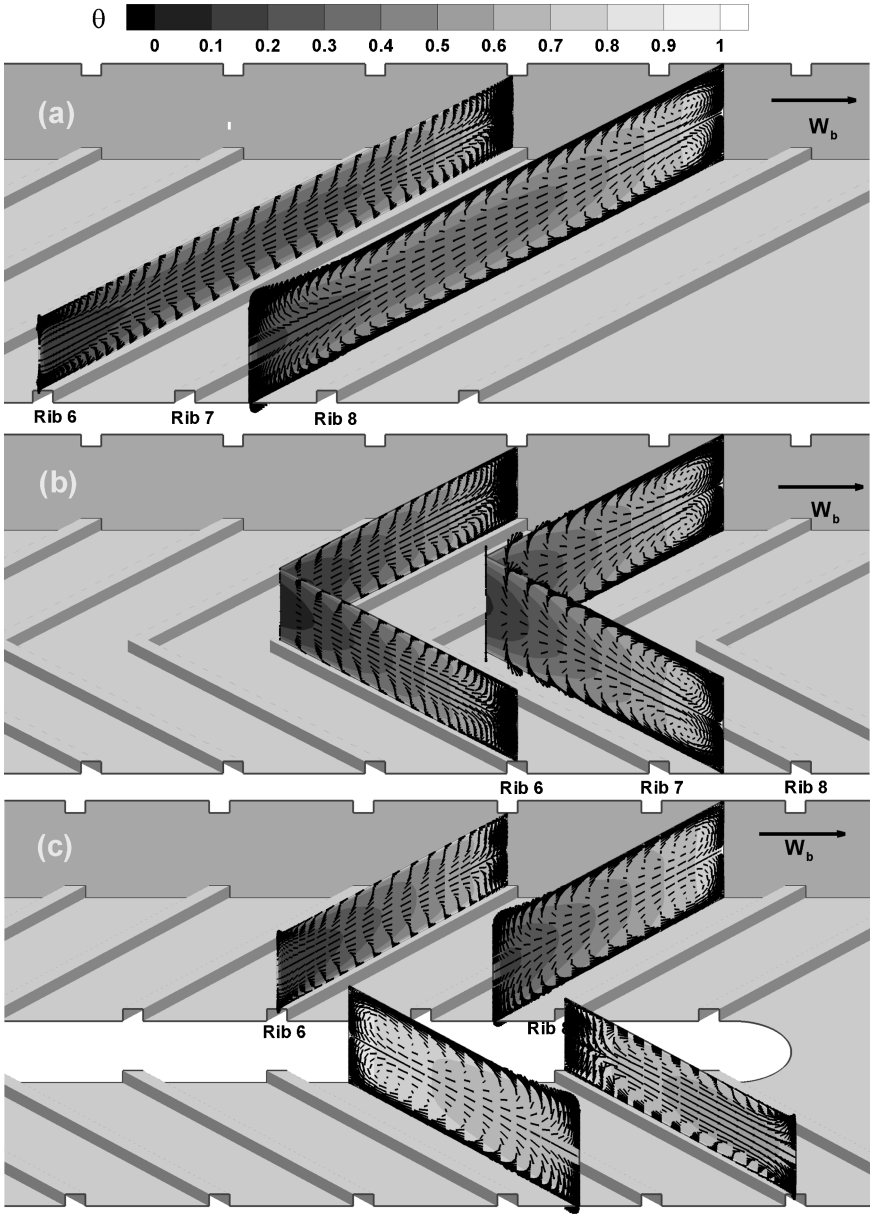

Fig. 12 Secondary flow vectors and temperature contours: a) AR = 4:1 one-pass channel with 45-deg inclined ribs, b) AR = 4:1 one-pass channel with V-shaped ribs, and c) AR = 2:1 two-pass channel with 45-deg inclined ribs ($Re = 10^4$).

channel with V-shaped ribs as obtained by Su et al.[73] Unlike the 45-deg inclined ribs, which move the secondary flow from one side of the channel to the other side along the ribbed surface, the V-shaped ribs direct the secondary flow from the center of the channel along the ribbed surfaces toward the side walls. When compared to the 45-deg inclined rib cases, the coolant in the core region of the V-shaped rib channel travels a shorter distance before impinging on the side walls, as seen in Fig. 12b. Further note that the shorter V-shaped ribs induce two pairs of vortices, which are considerably stronger than the single vortex pair induced by the longer 45-deg inclined ribs. Consequently, the coolant temperature in the V-shaped ribbed channel is significantly lower and more uniform in the core region of the channel. This leads to better overall heat transfer enhancement in comparison with the 45-deg inclined ribs for the same aspect ratio duct.

Figure 11c shows the secondary flow for nonrotating two-pass AR = 2:1 duct in the interrib regions near the trailing surface. The rib-induced vortex pairs on top of the rib and between the ribs are also shown in Fig. 12c to facilitate a direct comparison with those observed in the AR = 4:1 channels with 45-deg angled and V-shaped ribs. Note that the parallel angled ribs produce symmetric counter-rotating vortices that impinge on the inner surface in the first passage. The situation is reversed in the second passage, where the cooler fluid impinges on the outer surface. Note that the secondary flow and the corresponding temperature contours in the first passage of the AR = 2:1 channel are very similar to those observed in the upper-half of the AR = 4:1 channel with V-shaped ribs. However, the secondary flow in the second passage is drastically different from that in the lower-half of the V-shaped ribbed channel because the streamwise flow direction is reversed in the second passage after the 180-deg bend.

Figure 13 shows the dimensionless temperature contour and the vector field for $Re = 1 \times 10^4$ cases at a cross section midway between ribs 6 and 7 in the first passage for five different aspect ratio nonrotating ducts. Moreover, the Nusselt number ratios on all four walls are also shown in Fig. 13 to facilitate a detailed understanding of the heat transfer characteristics in different aspect ratio channels. As noted earlier, the effect of secondary flow on the temperature field is convecting the cooler fluid from the inner surface and along the ribbed surfaces toward the outer surface. The cooler fluid then moves back to the inner surface, which results in steep temperature gradients and high heat transfer coefficients on both

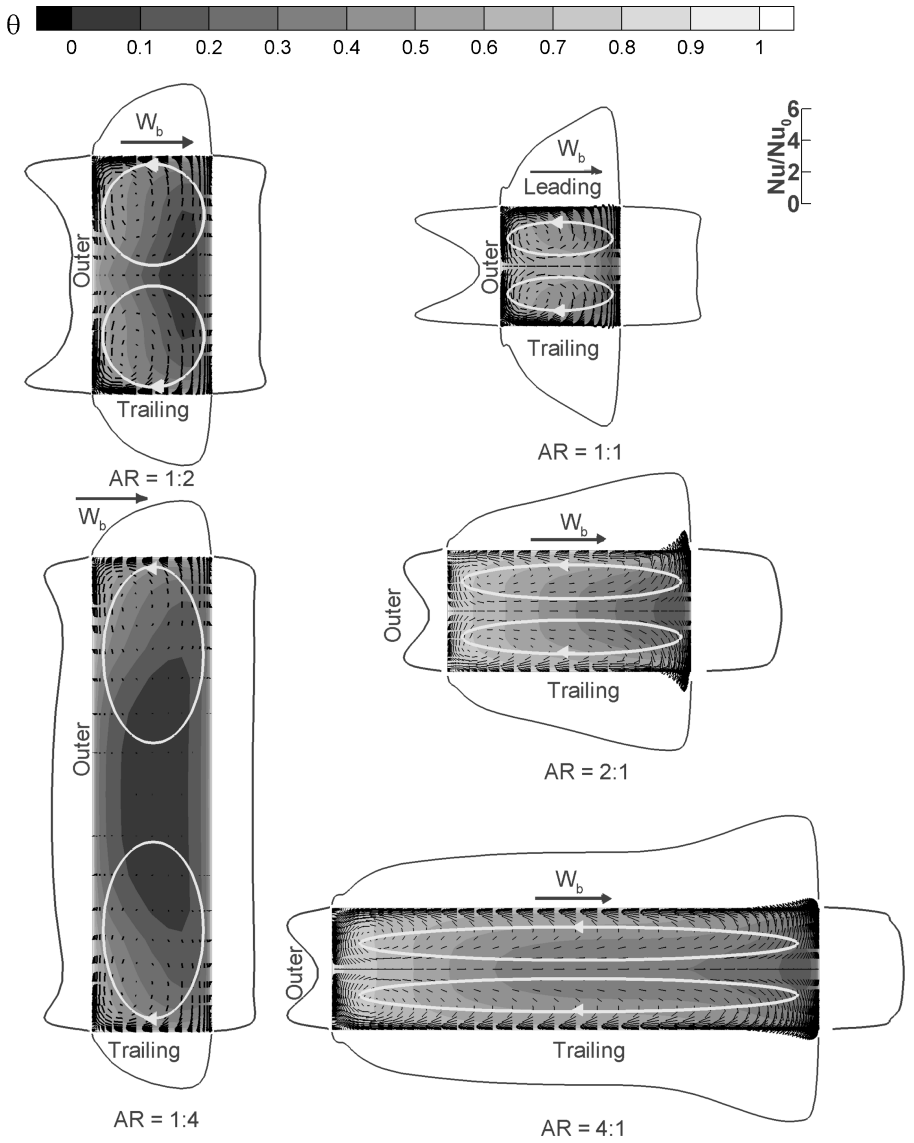

Fig. 13 Rib-induced secondary flows and temperature contours in the first passage (before the 180-deg turn) of non-rotating rectangular ducts ($Re = 10^4$).

the inner surface and the ribbed walls, as seen in the temperature contours and Nusselt number ratio curves. For the square and high aspect ratio channels, the rib-induced vortices occupy the entire channel. When the aspect ratio was reduced from $AR = 1{:}1$ to 1:4, the rib-induced vortices expand in the vertical direction. However, the strengths of the vortices become weaker in the lower aspect ratio channels. As noted earlier, the hydraulic diameter increases in lower aspect ratio channels because the channel height increases although the channel width and rib dimensions remain the same. Consequently, the rib height-to-hydraulic-diameter ratios (e/D_h) are smaller in the lower aspect channels. Furthermore, the inlet velocities in $AR = 1{:}2$ and 1:4 ducts are also reduced to only 75 and 62.5%, respectively, of that in the square ($AR = 1{:}1$) channel under the same Reynolds number condition. The combined effects of lower inlet velocity and smaller e/D_h has led to a significant drop of the Nusselt number ratios on the ribbed surfaces as the channel aspect ratio decreases.

Rotation-Induced Secondary Flow

In this section, we shall examine first the effects of rotation in smooth rectangular ducts without the additional complications due to the rib-induced secondary flows. The rotation effects in ribbed channels will be discussed in the next section. Figure 14 shows the cross-stream velocity vectors in the first passage for the rotating smooth ducts with rotation number $Ro = 0.22$ and density ratio $\Delta\rho/\rho = 0.22$. Under rotating conditions, the Coriolis forces in the first passage produce two counter-rotating vortices (stations A and B, Fig. 14), which pushes the cold fluid from the core toward the trailing surface and then brings it back along the inner and outer surfaces to the leading surface. This means that the thermal boundary layer starts at the trailing surface, grows along the two side surfaces, and ends at the leading surface. This results in small temperature gradient near the leading surface (hence, lower heat transfer coefficients) and steeper temperature gradient near the trailing surface (hence, higher heat transfer coefficients) as seen in the corresponding temperature contours in Fig. 14. Moreover, the cooler heavier fluid near the trailing surface will be accelerated by the centrifugal buoyancy force, whereas the hotter lighter fluid near the leading surface will be decelerated to maintain the continuity in the streamwise direction. The effects of centrifugal buoyancy force will be discussed in more detail later.

Before the sharp turn, the Coriolis-induced secondary flow is distorted slightly by the pressure gradient effect. In the middle of the turn, the two symmetric counter-rotating vortices induced by the 180-deg sharp turn (in the stationary case in Fig. 8) were found to be strongly distorted by rotation. This results into a considerable growth of the vortex near the leading surface at the expense of the one next to the trailing surface, which becomes weaker and moves

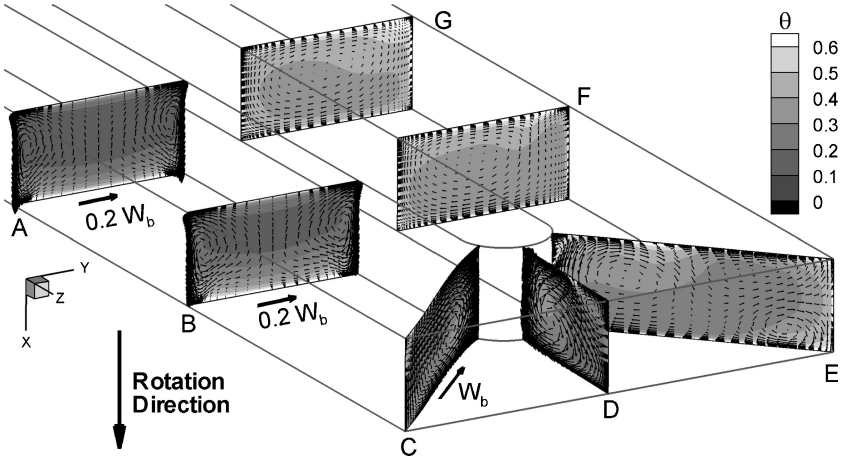

Fig. 14 Secondary flow and temperature contours in rotating AR = 2:1 smooth duct ($Re = 10^4$ and $Ro = 0.22$).

toward the outer surface. This leads to a considerable growth of the vortex near the leading surface at the expense of the one next to the trailing surface, which becomes weaker and moves toward the outer surface. This combined effect of the rotation- and turn-induced secondary flows push the cold fluid toward the outer surfaces as seen in the temperature contour plots at stations D and E. The rotation-induced secondary flow persists in the second passage for a considerable distance downstream of the turn as seen in stations F and G.

Figure 15 shows a comparison of the rotation-induced secondary flow in the first passage of five different aspect ratio ducts. The rotation number for the AR = 2:1 duct is $Ro = 0.11$, whereas a higher rotation number of $Ro = 0.14$ was used for the remaining four ducts. Unlike the rib-induced vortices, which are confined to the leading and trailing surfaces in low aspect ratio ducts, the rotation-induced vortices always occupy the entire duct regardless of the channel aspect ratio. This is to be expected because the Coriolis force acts on all fluid particles in the rectangular channel. For the AR = 2:1 duct, the rotation-induced vortices are nearly circular. As the channel aspect ratio is increased to AR = 4:1, the vortex pair expands horizontally to cover the entire trailing and leading surfaces and the heat transfer is enhanced almost uniformly over the entire trailing surface. For the square (AR = 1:1) and low aspect ratios (AR = 1:2 and 1:4), however, the rotation-induced vortices are squeezed in the horizontal direction. Also, the rotation-induced vortices grow considerably stronger in the AR = 1:4 duct because the secondary flow can be accelerated by the Coriolis force over a longer distance when the coolant travels from the leading surface to trailing surface. Consequently, the Nusselt number increases on the trailing surface and reduces on the leading surface as the channel aspect ratio reduces to AR = 1:4. Finally, note that the rotation-induced secondary flow is perpendicular to the rib-induced secondary flow shown in the preceding section.

Rotation- and Bend-Induced Secondary Flows

For completeness, the secondary flows in the midsection of the 180-deg turn of rotating smooth ducts are also shown in Fig. 16 for four different aspect ratio ducts to illustrate the combined effects of the rotation and bend-induced secondary flows on the heat transfer characteristics. Note that the bend-induced secondary flow is perpendicular to the Coriolis-induced secondary flow. In the bend, the vortex pair formed in the first passage by the channel rotation is overpowered by the bend-induced vortices. The combined effects of the rotation- and turn-induced vortices increase the strength and size of the vortex near the leading surface and reduce the size of the second vortex next to the trailing surface. Consequently, the cooler fluid is pushed toward the corner of the trailing and outer surfaces as shown in the corresponding temperature contours in Fig. 16.

Effects of Density Ratio

In addition to the Coriolis force, the channel rotation also induces centrifugal forces, which increase with the rotating arm length in the radial direction. For constant density flows, the centrifugal force terms can be analytically removed from the momentum equations by subtracting the rotation-induced centrifugal pressure terms from the total pressure. For rotating channel flows considered here, however, the coolant density is inversely proportional to the coolant temperature. This results in a net centrifugal buoyancy force on the coolant flow because the centrifugal force tends to accelerate the cooler fluid more than the hotter fluid. The centrifugal buoyancy force is proportional to the coolant temperature difference, which can be represented by the wall-to-coolant density ratio. Figure 17 shows the effect of centrifugal buoyancy force on the streamwise flow development for a smooth square duct as tested by Wagner et al.[19] As noted in Chen et al.,[76,77] the Coriolis and centrifugal buoyancy forces produced a region of axial flow reversal at the end of the first passage near the inner surface. The Coriolis forces push the cold and heavy fluid toward the trailing surface so that the centrifugal buoyancy force tends to slow down the hotter and lighter fluid, producing thicker boundary layer near the leading surface, and accelerates the heavier fluid near the trailing surface. Thus, it causes flow reversal in the streamwise direction on the leading surface as shown in Figs. 17b and 17c. The size of the reverse flow region depends on the magnitude of the buoyant force, but so far, no measurement provides the magnitude or extent of the reverse flow.

Rotation- and Rib-Induced Secondary Flows

After examining the secondary flows induced by the channel rotation and rib turbulators separately, it is desirable to investigate also the combined effects of rib- and rotation-induced secondary flows in the first passage of rotating ribbed channels. Before the detailed flowfield is discussed, a general conceptual view about the secondary flow patterns induced by angled ribs and rotation is shown in Fig. 18. The parallel angled ribs in the nonrotating duct (Fig. 18a) produce symmetric counter-rotating vortices that impinge on the inner surface in the first passage and on the outer surface in the second passage. The Coriolis force in the 90-deg rotating duct (Fig. 18b) produces two additional counter-rotating vortices that push the cooler fluid from the core to the trailing surface in the first passage and to the leading surface in the second passage. For the 135-deg rotating duct (Fig. 18c), the Coriolis force produces secondary flow that migrates diagonally away from the corner of the inner-leading surfaces toward the center of the channel in the first passage and from the corner of the inner-trailing surfaces toward the center of the channel in the second passage.

Figure 19 shows the secondary flow induced by the combined effects of channel rotation and 45-deg inclined ribs for five different

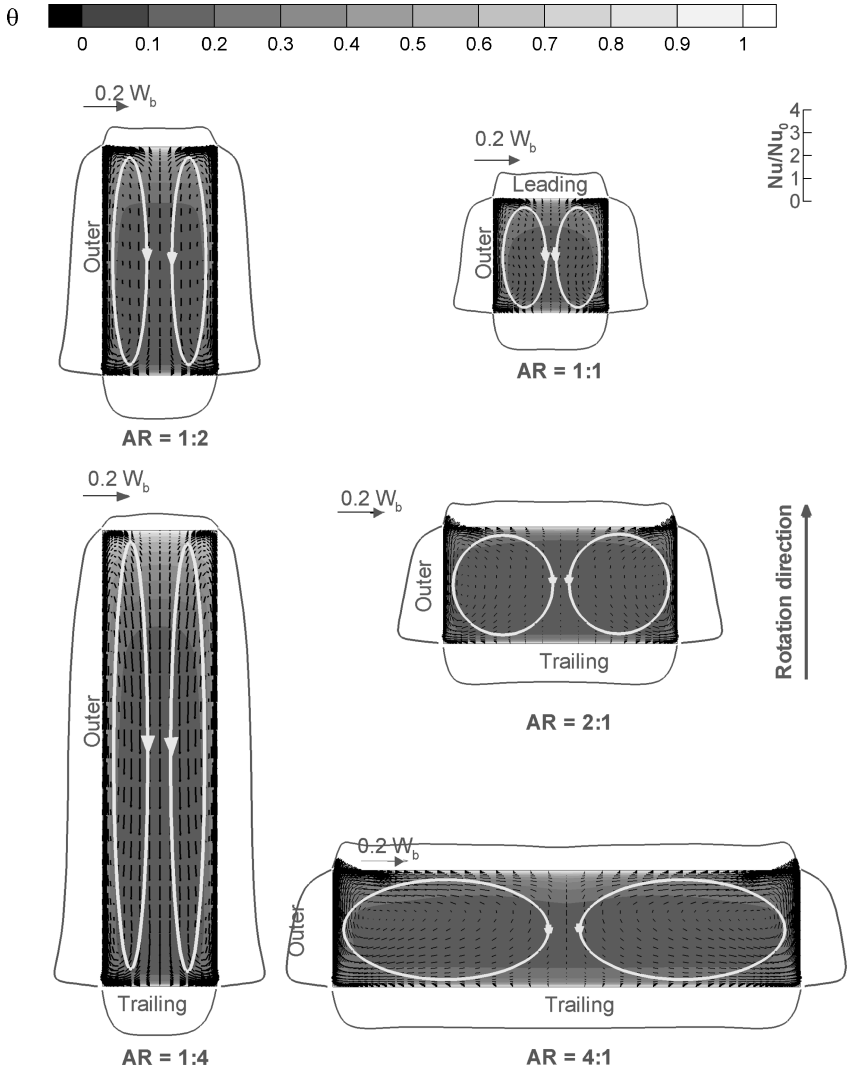

Fig. 15 Temperature contours and secondary flow in first passage of rotating channels with different aspect ratios ($Re = 10^4$, $Ro = 0.11$ for AR = 2:1 duct and 0.14 for the other four ducts).

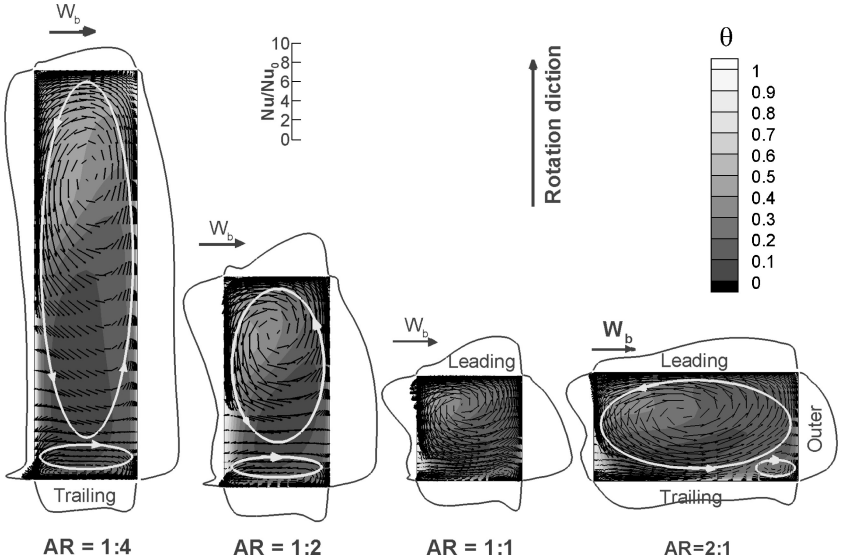

Fig. 16 Secondary flows and temperature contours in midsection of the bend of rotating smooth channels ($Re = 10^4$, $Ro = 0.11$ for AR = 2:1 channel and 0.14 for the other three cases).

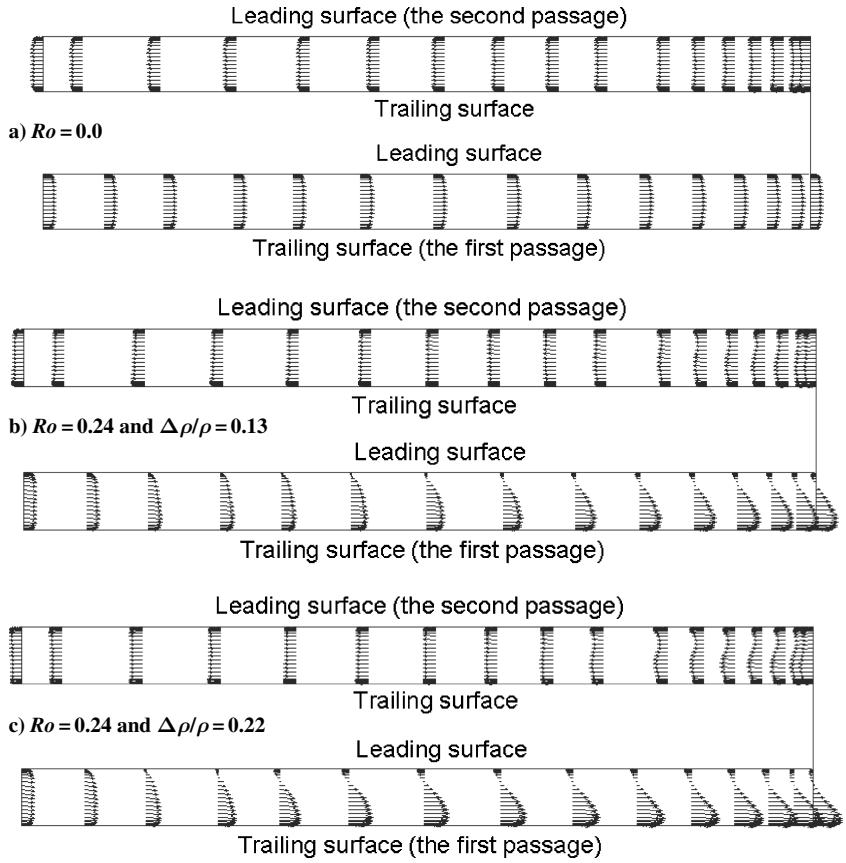

Fig. 17 Velocity vectors midway between inner and outer surfaces of smooth square duct (Chen et al.[77]).

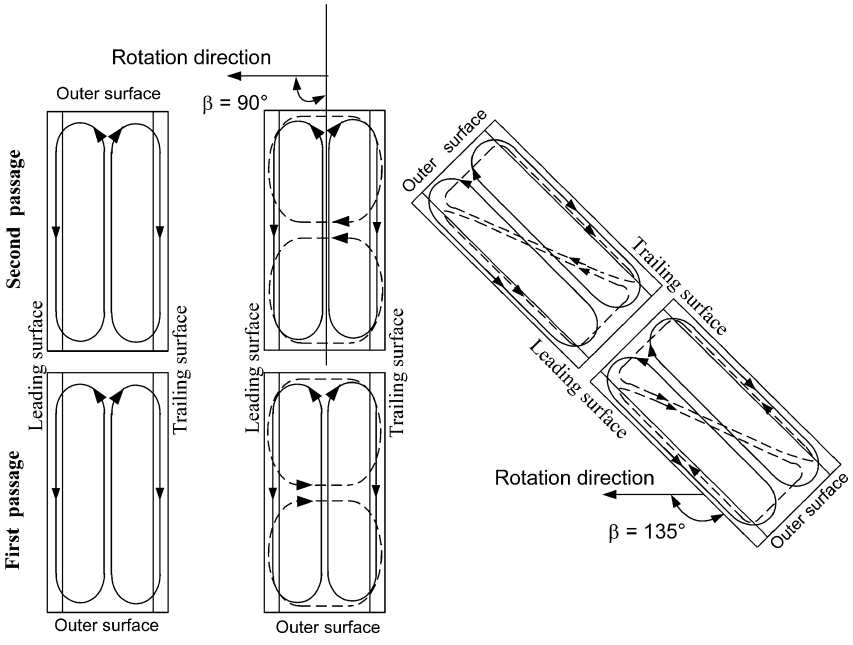

a) Nonrotating, $Ro = 0.0$, and $\Delta\rho/\rho = 0.115$ **b) Rotating, $Ro = 0.11$, $\Delta\rho/\rho = 0.115$, and $\beta = 90$ deg** **c) Rotating, $Ro = 0.11$, $\Delta\rho/\rho = 0.115$, and $\beta = 135$ deg**

Fig. 18 Secondary flow induced by angled ribs and rotation (Al-Qahtani et al.[84]): - - - - -, rotation-induced secondary flow and ———, rib-induced secondary flow.

aspect ratio channels at a station between ribs 7 and 8 in the first passage before the 180-deg turn. As noted earlier, the rotation number for the AR = 2:1 duct ($Ro = 0.11$) is somewhat lower than that used in the other four ducts ($Ro = 0.14$). In all five channels, the Coriolis forces produce a pair of counter-rotating vortices, which moves cooler fluids in the core region toward the trailing surface. When compared to the nonrotating cases shown in Fig. 13, note that the symmetric vortices induced by the inclined ribs were significantly modified by the channel rotation. The rib-induced vortex near the trailing surface was expanded to occupy a large portion of the channel, whereas the vortex near the leading surface was suppressed. This effect is more pronounced in the low aspect ratio ducts. Al-Qahtani et al.[70] and Su et al.[75] also compared the secondary flow vectors and temperature contours in the bend region and the second passage for different aspect ratio rectangular channels. They found that the secondary flow structures are significantly modified by the

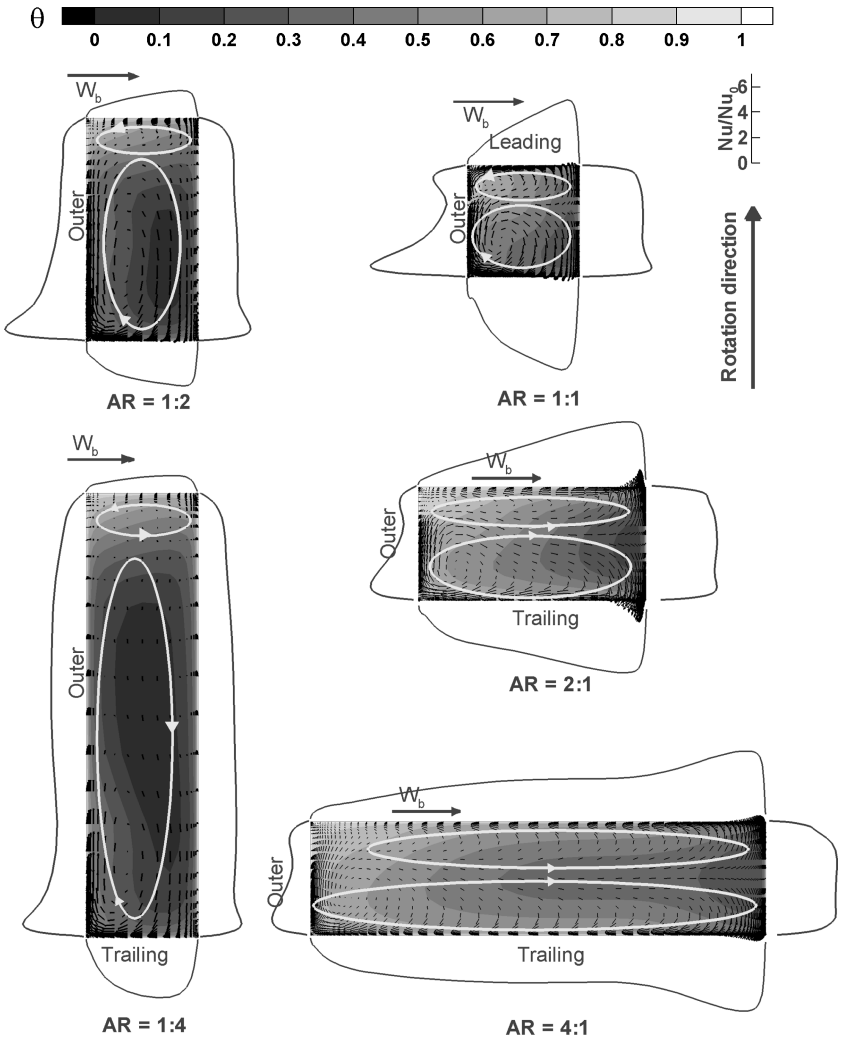

Fig. 19 Secondary flow in first passage (before the 180-deg turn) of rotating ribbed channels with different aspect ratios ($Re = 10^4$ and $Ro = 0.14$).

180-deg sharp turn. In the bend region, the rotation- and rib-induced vortices in the first passage were combined with the much stronger bend-induced vortices to form a large vortex near the leading surface and a smaller vortex adjacent to the trailing surface. In the second passage, the Coriolis force acts in the opposite direction and pushes the cold fluid toward the leading surface. Consequently, the vortex induced by the rib near the leading surface was enlarged and the vortex near the trailing surface was reduced.

Effects of Channel Orientation

Because of the aerodynamic shape of the turbine blade, the orientation of the cooling channel in the leading- and trailing-edge regions of the turbine blade may be at an angle β (Fig. 7) from the direction of rotation, and its cross section may not be square. In addition to the aspect ratio effects discussed earlier, it is also desirable to investigate the effect of channel orientation on the secondary flow structure and the corresponding heat transfer enhancement. Al-Qahtani et al.[70,71,84] computed the flow and heat transfer for AR = 2:1 and 4:1 rectangular channels with either smooth walls or 45-deg angled ribs at a channel orientation of $\beta = 135$ deg. Su et al.[73] also investigated the effect channel orientation for AR = 4:1 rectangular duct with V-shaped ribs at $\beta = -135$ deg and 135 deg. In Fig. 20, the local Nusselt number ratio contours on the leading and trailing surfaces for the nonrotating (case 1) and rotating ribbed channels with two different orientations of $\beta = 90$ deg (case 2) and 135 deg (case 3) are compared, respectively. For the nonrotating case shown in Figs. 20a and 20b, the highest Nusselt number ratios were obtained on the top of the ribs, and the lower Nusselt number ratios were obtained right before and after the ribs. Between any two ribs in the first passage, the Nusselt number ratios are highest near the inner surface and decrease as we move toward the outer surface. This is due to the rib-induced secondary flow moving from the rib leading to the trailing side as shown in Fig. 18a. Nusselt number ratios in the turn are higher in the region next to the divider wall tip while lower at the first corner. In the second passage (between any two ribs), the Nusselt number ratios are higher near the outer surface and decrease as we move toward the inner surface. Again, this is a result of the rib-induced secondary flow in the second passage shown in Fig. 18b, Figures. 20c and 20e show the Nusselt number ratio contours on the leading side for case 2 ($Ro = 0.11$ and $\beta = 90$ deg), and case 3 ($Ro = 0.11$ and $\beta = 135$ deg), respectively. Comparing Figs. 20c and 20e with the nonrotating leading side, we notice that the Nusselt number ratios decrease in the first passage, in both cases, with the decrease in case 3 being higher. In the second passage, the Nusselt number ratios in both cases increase with respect to case 1. Figures 20d and 20f show the Nusselt number ratios contours on the trailing surface for case 2 ($Ro = 0.11$ and $\beta = 90$ deg) and case 3 ($Ro = 0.11$ and $\beta = 135$ deg), respectively. Comparing Figs. 20d and 20f with the nonrotating trailing side, we notice that the Nusselt number ratios increase in the first passage, for both cases, with the increase in case 2 being higher. In the second passage, the Nusselt number ratios in both cases decrease slightly, with the decrease in case 2 being higher. The Nusselt number in the bend is much higher for both cases when compared to the nonrotating case.

Effects of Rib Configuration

In addition to the 45-deg angled ribs, Jang et al.[85,86,69] also presented numerical results for square channels with 90- and 60-deg

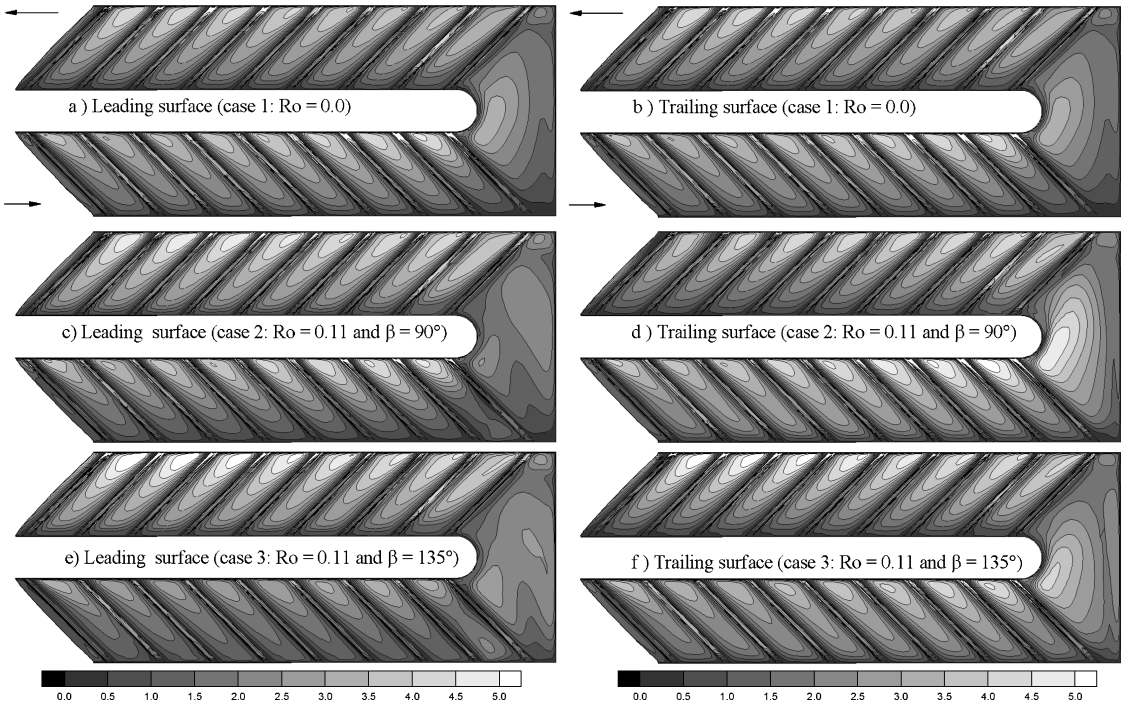

Fig. 20 Detailed Nusselt number ratios for AR = 2:1 rectangular duct (Al-Qahtani et al.[70]).

angled ribs, and 45-deg ribs with rounded cross section, respectively. It is worthwhile to examine the effects of rib angle and rib shape on the secondary flow pattern and heat transfer enhancement. As noted by Jang et al.,[85] the 90-deg parallel-ribbed channel produced periodic separation and reattachment flow pattern and simultaneously generated small corner vortices near the bottom surface on both the inner and outer surfaces. On the other hand, the secondary flow induced by the 60-deg angled ribs (see Jang et al.[86]) is similar to that induced by the 45-deg angled ribs. In general, the angled ribs produced significantly higher heat transfer enhancement than the 90-deg normal ribs. The predicted Nusselt number ratios shown in Jang et al.[85,86] for the 90- and 60-deg ribbed channels, respectively, are in good agreement with corresponding experimental data of Ekkad and Han.[87]

Jang et al.[69] also computed the flow and heat transfer in square channel with 45-deg angled ribs of rounded cross section as tested by Johnson et al.[20] Figure 21a shows the streamwise velocity vector distribution for nonrotating square channel with rounded 45-deg ribs at three locations: in the middle of the rib, near the inner surface ($0.018D_h$ from the inner surface), and near the outer surface ($0.018D_h$ from the outer surface). Flow separation was present near the inner surface but not at the middle of the ribs or near the outer surface. The rounded rib shape tends to reduce the extent of flow separation as compared to the sharp rectangular ribs. Figure 21b shows the streamwise velocity vector distribution for the entire section of the plane between the leading and trailing surfaces in the middle of the ribs at a rotation number of 0.24 and inlet density ratio of 0.13. Unlike the nonrotating case, flow separation was present on the leading surface due to the centrifugal buoyancy force, which tended to slow down the lighter fluid (lower density fluid) near the leading surface. Also observe that the high-momentum cooler fluid was pushed toward the trailing surface by the Coriolis forces.

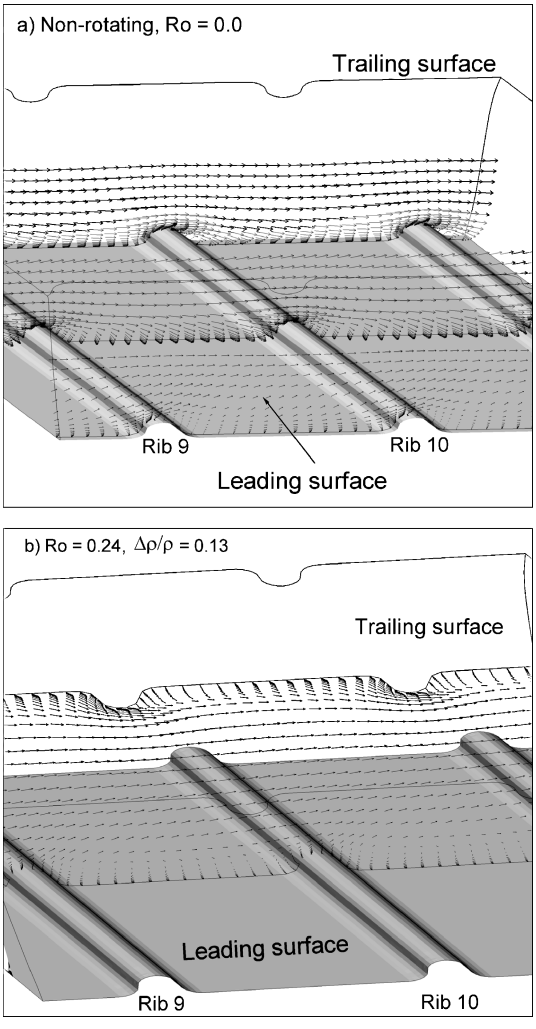

Fig. 21 Streamwise velocity vectors for 45-deg ribbed duct: a) *Ro* = 0 and b) *Ro* = 0.24 (Jang et al.[69]).

High Reynolds Number High Rotation Number and High Density Ratio Effects

In addition to the simulation of flow and heat transfer fields for various smooth and ribbed channel configurations corresponding to typical experimental conditions, it is quite straightforward to extend the present near-wall second-moment RANS method for the

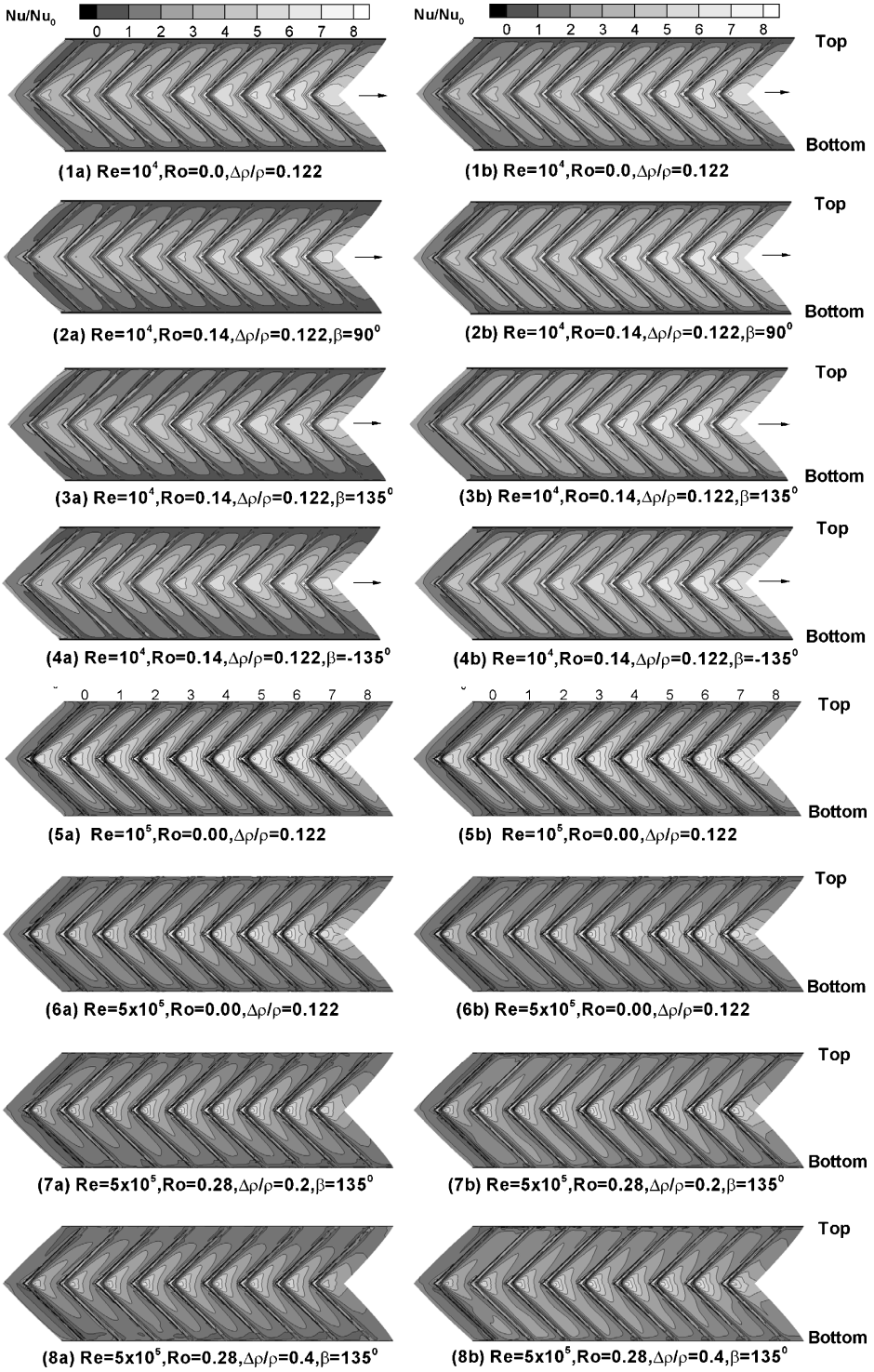

Fig. 22 Nusselt number ratio contours for AR = 4:1 channel with 45-deg V-shaped ribs (Su et al.[73]): a) leading and b) trailing surface.

investigation of heat transfer enhancement under high Reynolds number, high rotation number, and high wall-to-coolant density ratio flow conditions, which are closer to engine conditions. In this respect, the numerical simulation enables us to cover a much wider range of design parameters, which may be difficult to attain in experimental investigations. In recent studies by Su et al.,[73–75] calculations were performed for rotating rectangular channels with Reynolds number up to 5×10^5, rotating number up to 0.28, and density ratio up to 0.4. Figure 22 shows the local Nusselt number ratio contours on the leading and trailing surfaces for AR = 4:1 rectangular channel with V-shaped ribs for eight different test cases to facilitate a detailed assessment on the effects of Reynolds number and rotation. When the Reynolds number was increased from 10^4 to 10^5 and 5×10^5, the Nusselt number ratio in the middle section of the channel decreases significantly, indicating that the heat transfer enhancement caused by the rib-induced secondary flow is reduced when the thermal boundary layer becomes thinner at high Reynolds numbers. However, note that the actual Nusselt numbers are much higher for the high Reynolds number cases because the Nusselt number Nu_o for smooth duct (proportional to $Re^{0.8}$) is already very high in these cases due to high turbulence and high-temperature gradient inside the boundary layer.

A comparison between Fig. 22(6), the high Re non-rotating case, and Fig. 22(7), the high Reynolds number and high rotation number case, shows that channel rotation leads to a significant decrease in Nusselt number ratio on the leading surface. On the other hand, the

Nusselt number ratios on the trailing surface increase slightly due to the effect of channel rotation. Also note that the high Nusselt number ratio regions on the trailing surface spread toward the side walls. This is due to the rotation-induced secondary flow that pushes the cooler fluid toward the trailing surface and side walls. In cases shown in Figs. 22(7) and 22(8), the density ratio is increased from 0.20 to 0.40, whereas the Reynolds number and rotation number are kept the same. It is quite clear that an increase in density ratio leads the Nusselt number ratios to further decrease on the leading surface and slightly decrease on the trailing surface. This is because an increased density ratio intensifies the effect of the rotation-induced Coriolis force. On the trailing surface, the combined effects of rotation and higher density ratio tend to offset each other, but the total effect is still to increase the Nusselt number ratios on the trailing surface. As the density ratio increases from 0.2 to 0.4, significant enhancements in Nusselt number ratios are observed on the top and bottom surfaces.

Summary

Most experimental data available to date are for rotating rectangular cooling channels with high-performance rib turbulators for Reynolds number up to 5×10^4 rotation number up 0.25, and buoyancy parameter up to 0.5. More studies are needed for the blade-shaped coolant passages (realistic cooling passage geometry, shape, and orientation) with high-performance turbulators and with or without film cooling holes under higher coolant flow (Reynolds number up to 5×10^5), thermal (buoyancy parameter up to 5), and rotation (rotation number up to 0.5) conditions. Highly accurate and highly detailed local heat transfer coefficient and pressure drop data under these extreme cooling design conditions would be needed to prevent the blade from failure due to local hot spots. Also, more studies are needed for rotating impingement cooling with or without film coolant extraction, as well as rotating pin-fin cooling with or without trailing-edge ejection to guide efficient rotor blade internal cooling designs. Heat transfer enhancement vs pressure drop penalty should continue to identify the best heat transfer augmentation technique including compound and new cooling techniques. Development of accurate and efficient CFD prediction tools should continue to provide valuable information for designing effective cooled rotor blades for the new generation of gas turbines.

References

[1]Dutta, S., and Han, J. C., "Rotational Effect on the Turbine Blade Coolant Passage Heat Transfer," *Annual Review of Heat Transfer*, Vol. 9, 1998, pp. 269–314.

[2]Han, J. C., "Recent Studies in Turbine Blade Cooling," *Proceedings of the 9th International Symposium on Transport Phenomena and Dynamics of Rotating Machinery* (ISROMAC-9), Invited Lecture-5, 2002.

[3]Han, J. C., and Dutta, S., "Recent Developments in Turbine Blade Internal Cooling," *Heat Transfer in Gas Turbine Systems*, edited by R. J., Goldstein, Vol. 934, Annals of the New York Academy of Sciences, New York, 2001, Vol. 934, pp. 162–178.

[4]Han, J. C., Dutta, S., and Ekkad, S. V., *Gas Turbine Heat Transfer and Cooling Technology*, Taylor and Francis, New York, 2000, pp. 1–646.

[5]Goldstein, R. J., *Heat Transfer in Gas Turbine Systems*, Vol. 934, Annals of the New York Academy of Sciences, New York, 2001, pp. 1–520.

[6]Dunn, M. G., "Convection Heat Transfer and Aerodynamics in Axial Flow Turbines," *Journal of Turbomachinery*, Vol. 123, 2001, No. 4, pp. 637–686.

[7]Han, J. C., Glicksman, L. R., and Rohsenow, W. M., "An Investigation of Heat Transfer and Friction for Rib-Roughened Surfaces," *International Journal of Heat and Mass Transfer*, Vol. 21, 1978, pp. 1143–1156.

[8]Han, J. C., Park, J. S., and Lei, C. K., "Heat Transfer Enhancement in Channels with Turbulence Promoters," *Journal of Engineering for Gas Turbines and Power*, Vol. 107, No. 1, 1985, pp. 628–635.

[9]Han, J. C., "Heat Transfer and Friction Characteristics in Rectangular Channels with Rib Turbulators," *Journal of Heat Transfer*, Vol. 110, No. 2, 1988, pp. 321–328.

[10]Han, J. C., and Park, J. S., "Developing Heat Transfer in Rectangular Channels with Rib Turbulators," *International Journal of Heat and Mass Transfer*, Vol. 31, No. 1, 1988, pp. 183–195.

[11]Han, J. C., Ou, S., Park, J. S., and Lei, C. K., "Augmented Heat Transfer in Rectangular Channels of Narrow Aspect Ratios with Rib Turbulators," *International Journal of Heat and Mass Transfer*, Vol. 32, No. 9, 1989, pp. 1619–1630.

[12]Han, J. C., and Zhang, P., "Effect of Rib Angle Orientation on Local Mass Transfer Distribution in a Three-Pass Rib-Roughened Channel," *Journal of Turbomachinery*, Vol. 113, 1991, pp. 123–130.

[13]Han, J. C., and Zhang, Y. M., "High Performance Heat Transfer Ducts with Parallel and V-Shaped Broken Ribs," *International Journal of Heat and Mass Transfer*, Vol. 35, No. 2, 1992, pp. 513–523.

[14]Han, J. C., Huang, J. J., and Lee, C. P., "Augmented Heat Transfer in Square Channels with Wedge-Shaped and Delta-Shaped Turbulence Promoters," *Journal of Enhanced Heat Transfer*, Vol. 1, No. 1, 1993, pp. 37–52.

[15]Ekkad, S. V., Huang, Y., and Han, J. C., "Detailed Heat Transfer Distributions in Two-Pass Smooth and Turbulated Square Channels with Bleed Holes," *International Journal of Heat and Mass Transfer*, Vol. 41, No. 13, 1998, pp. 3781–3791.

[16]Taslim, M. E., and Wadsworth, C. M., "An Experimental Investigation of the Rib Surface-Averaged Heat Transfer Coefficient in a Rib-Roughened Square Passage," *Journal of Turbomachinery*, Vol. 119, No. 2, 1997, pp. 381–389.

[17]Taslim, M. E., and Lengkong, A., "45-Degree Round-Corner Rib Heat Transfer Coefficient Measurements in a Square Channel," American Society of Mechanical Engineers, ASME Paper 98-GT-176, June 1998.

[18]Taslim, M. E., and Lengkong, A., "45-Degree Staggered Rib Heat Transfer Coefficient Measurements in a Square Channel," *Journal of Turbomachinery*, Vol. 120, No. 3, 1998, pp. 571–580.

[19]Wagner, J. H., Johnson, B. V., and Kopper, F. C., "Heat Transfer in Rotating Serpentine Passages with Smooth Walls," *Journal of Turbomachinery*, Vol. 113, No. 3, 1991, pp. 321–330.

[20]Johnson, B. V., Wagner, J. H., Steuber, G. D., and Yeh, F. C., "Heat Transfer in Rotating Serpentine Passages with Trips Skewed to the Flow," *Journal of Turbomachinery*, Vol. 116, No. 1, 1994, pp. 113–123.

[21]Han, J. C., Zhang, Y. M., and Kalkuehler, K., "Uneven Wall Temperature Effect on Local Heat Transfer in Rotating Two-Pass Square Channel with Smooth Walls," *Journal of Heat Transfer*, Vol. 114, No. 4, 1993, pp. 850–858.

[22]Parsons, J. A., Han, J. C., and Zhang, Y. M., "Wall Heating Effect on Local Heat Transfer in a Rotating Two-Pass Square Channel with 90-Degree Rib Turbulators," *International Journal of Heat and Mass Transfer*, Vol. 37, No. 9, 1994, pp. 1411–1420.

[23]Zhang, Y. M., Han, J. C., Parsons, J. A., and Lee, C. P., "Surface Heating Effect on Local Heat Transfer in a Rotating Two-Pass Square Channel with 60-Degree Angled Rib Turbulators," *Journal of Turbomachinery*, Vol. 117, No. 2, 1995, pp. 272–278.

[24]Johnson, B. V., Wagner, J. H., Steuber, G. D., and Yeh, F. C., "Heat Transfer in Rotating Serpentine Passages with selected Model Orientations for Smooth or Skewed Tip Walls," *Journal of Turbomachinery*, Vol. 116, No. 4, 1994, pp. 738–744.

[25]Parsons, J. A., Han, J. C., and Zhang, Y. M., "Effects of Model Orientation and Wall Heating Condition on Local Heat Transfer in a Rotating Two-Pass Square Channel with Rib Turbulators," *International Journal of Heat and Mass Transfer*, Vol. 38, No. 7, 1995, pp. 1151–1159.

[26]Dutta, S., and Han, J. C., "Local Heat Transfer in Rotating Smooth and Ribbed Two-Pass Square Channels with Three Channel Orientations," *Journal of Heat Transfer*, Vol. 118, No. 3, 1996, pp. 578–584.

[27]Al-Hadhrami, L., and Han, J. C., "Effect of Rotation in Two-Pass Square Channels with Parallel and Crossed 45 angled Rib Turbulators," 9th International Symposium on Transport Phenomena and Dynamics of Rotating Machinery, ISROMAC-9, Rept. HT-ABS-031, March 2002; also *International Journal of Heat and Mass Transfer*, Vol. 46, Feb. 2003, pp. 653–669.

[28]Clifford, R. J., Morris, W. D., and Harasgama, S. P., "An Experimental Study of Local and Mean Heat Transfer in a Triangular-Sectioned Duct Rotating in the Orthogonal Mode," *Journal of Engineering for Gas Turbines and Power*, Vol. 106, No. 3, 1984, pp. 661–667.

[29]Harasgama, S. P., and Morris, W. D., "The Influence of Rotation on the Heat Transfer Characteristics of Circular, Triangular, and Square-Sectioned Coolant Passages of Gas Turbine Rotor Blades," *Journal of Turbomachinery*, Vol. 110, No. 1, 1988, pp. 44–50.

[30]Dutta, S., Han, J. C., Zhang, Y. M., and Lee, C. P., "Local Heat Transfer in a Rotating Two-Pass Triangular Duct with Smooth Walls," *Journal of Turbomachinery*, Vol. 118, No. 3, 1996, pp. 435–443.

[31]Dutta, S., Han, J. C., and Lee, C. P., "Local Heat Transfer in a Rotating Two-Pass Ribbed Triangular Duct with Two Model Orientations," *International Journal of Heat and Mass Transfer*, Vol. 39, No. 4, 1996, pp. 707–715.

[32]Guidez, J., "Study of the Convective Heat Transfer in a Rotating Coolant Channel," *Journal of Turbomachinery*, Vol. 111, No. 1, 1989, pp. 43–50.

[33]Soong, C. Y., Lin, S. T., and Hwang, G. J., "An Experimental Study of Convective Heat Transfer in Radially Rotating Rectangular Ducts," *Journal of Heat Transfer*, Vol. 113, No. 3, 1991, pp. 604–611.

[34]Taslim, M. E., Bondi, L. A., and Kercher, D. M., "An Experimental Investigation of Heat Transfer in an Orthogonally Rotating Channel Roughened with 45 Deg Criss-Cross Ribs on Two Opposite Walls," *Journal of Turbomachinery*, Vol. 113, 1991, pp. 346–353.

[35] Azad, G. S., Uddin, J. M., Han, J. C., Moon, H. K., and Glezer, B., "Heat Transfer in a Two-Pass Rectangular Rotating Channel with 45-Degree Angled Rib Turbulators," American Society of Mechanical Engineers, ASME Paper 2001-GT-186, June 2001, also *Journal of Turbomachinery*, Vol. 124, April 2002, pp. 251–259.

[36] Al-Hadhrami, L., Griffith, T. S., and Han, J. C., "Heat Transfer in Two-Pass Rotating Rectangular Channels ($AR = 2$) with Parallel and Crossed 45° V-shaped Rib Turbulators," AIAA Paper 2002-0789, 2002; also *Journal of Heat Transfer*, Vol. 125, No. 2, 2003, pp. 232–242.

[37] Griffith, T. S., Al-Hadhrami, L., and Han, J. C., "Heat Transfer in Rotating Rectangular Cooling Channels ($AR = 4$) with Angled Ribs," AIAA Paper 2001-2820, 2001; also *Journal of Heat Transfer*, Vol. 124, No. 4, 2002, pp. 617–625.

[38] Willett, F. T., and Bergles, A. E., "Heat Transfer in Rotating Narrow Rectangular Ducts with Heated Sides Oriented at 60-Degree to the R-Z Plane," American Society of Mechanical Engineers, ASME Paper 2000-GT-224, May 2000.

[39] Lee, E., Wright, L. M., and Han, J. C., "Heat Transfer in Rotating Rectangular Channels ($AR = 4{:}1$) with V-Shaped and Angled Rib Turbulators with and without Gaps," American Society of Mechanical Engineers, ASME Paper GT-2003-38900, June 2003.

[40] Acharya, S., Agarwal, P., and Nikitopoulos, D. E., "Heat/Mass Transfer in a 4:1 AR Smooth and Ribbed Coolant Passage with Rotation in 90-Degreee and 45-Degree Orientations," American Society of Mechanical Engineers, ASME Paper GT2004-53928, June 2004.

[41] Zhou, F., Lagrone, J., and Acharya, S., "Internal Cooling in 4:1 AR Passages at High Rotation Numbers," American Society of Mechanical Engineers, ASME Paper GT2004-53501, June 2004.

[42] Wright, L. M., Fu, W. L., and Han, J. C., "Thermal Performance of Angled, V-Shaped, and W-Shaped Rib Turbulators in Rotating Rectangular Cooling Channels ($AR = 4{:}1$)," American Society of Mechanical Engineers, ASME Paper GT2004-54073, June 2004.

[43] Agarwal, P., Acharya, S., and Nikitopoulos, D. E., "Heat/Mass Transfer in 1:4 Rectangular Passages with Rotation," American Society of Mechanical Engineers, ASME Paper GT2003-38615, June 2003.

[44] Cho, H. H., Kim, Y. Y., Kim, K. M., and Rhee, D. H., "Effects of Rib Arrangements and Rotation Speed on Heat Transfer in a Two-Pass Duct," American Society of Mechanical Engineers, ASME Paper GT2003-38609, June 2003.

[45] Kim, K. M., Kim, Y. Y., Rhee, D. H., and Cho, H. H., "An Investigation of Duct Aspect Ratio Effects on Heat/Mass Transfer in a Rotating Duct with 90° Ribs," American Society of Mechanical Engineers, ASME Paper GT2004-53533, June 2004.

[46] Fu, W. L., Wright, L. M., and Han, J. C., "Heat Transfer in Two-Pass Rotating Rectangular Channels ($AR = 1{:}2$ and $1{:}4$) with 45° Angled Rib Turbulators," American Society of Mechanical Engineers, ASME Paper GT2004-53261, June 2004.

[47] Fu, W. L., Wright, L. M., and Han, J. C., "Heat Transfer in Two-Pass Rotating Rectangular Channels ($AR = 1{:}2$ and $1{:}4$) with Smooth Walls," *Journal of Heat Transfer*, Vol. 127, March 2005.

[48] Rathjen, L., Hennecke, D. K., Bock, S., and Kleinstuck, R., "Detailed Heat/Mass Transfer Distributions in a Rotating Two Pass Coolant Channel with Engine-Near Cross Section and Smooth Walls," *Heat Transfer in Gas Turbine Systems*, edited by R. J., Goldstein, Vol. 934, Annals of the New York Academy of Sciences, New York, pp. 432–439.

[49] Lezius, D. K., and Johnston, J. P., "Roll-Cell Instabilities in Rotating Laminar and Turbulent Channel Flows," *Journal of Fluid Mechanics*, Vol. 77, 1976, pp. 153–175.

[50] Elfert, M., "The Effect of Rotation and Bouyancy on Flow Development in a Rotating Circular Coolant Channel," *Engineering Turbulence Modelling and Experiments 2*, edited by W. Rodi and F. Martelli, Elsevier, Amsterdam, 1993, pp. 815–824.

[51] Tse, D. G. N., and McGrath, D. B., "A Combined Experimental/Computational Study of Flow in Turbine Blade Cooling Passage. Part I: Experimental Study," American Society of Mechanical Engineers, ASME Paper 95-GT-355, June 1995.

[52] Tse, D. G. N., and Steuber, G. D., "Flow in a Rotating Square Serpentine Coolant Passage with Skewed Trips," American Sociey of Mechanical Engineers, ASME Paper 97-GT-529, 1997.

[53] Cheah, S. C., Iacovides, H., Jackson, D. C., Ji, H., and Launder, B. E., "LDA Investigation of the Flow Development through Rotating U-Ducts," *Journal of Turbomachinery*, Vol. 118, No. 3, 1996, pp. 590–595.

[54] Bons, J. P., and Kerrebrock, J. L., "Complementary Velocity and Heat Transfer Measurements in a Rotating Cooling Passage with Smooth Walls," American Society of Mechanical Engineers, ASME Paper 98-GT-464, June 1998.

[55] Schabacker, J., Bolcs, A., and Johnson, B. V., "PIV Investigation of the Flow Characteristics in an Internal Coolant Passage with 45° Rib Arrangement," American Society of Mechanical Engineers, ASME Paper GT99-120, June 1990.

[56] Chanteloup, D., Juaneda, Y., and Bolcs, A., "Combined 3D Flow and Heat Transfer Measurements in a 2-pass Internal Coolant Passage of Gas Turbine Airfoil," American Society of Mechanical Engineers, ASME Paper GT2002-30214, June 2002.

[57] Son, S. Y., Kihm, K. D., and Han, J. C., "PIV Flow Measurements for Heat Transfer Characterization in Two-Pass Square Channels with Smooth and 90-degree Ribbed Walls," *International Journal of Heat and Mass Transfer*, Vol. 45, No. 24, 2002, pp. 4809–4822.

[58] Liou, T. M., and Chen, C. C., "LDV Study of Developing Flows through a Smooth Duct with a 180 Deg Straight-Corner Turn," *Journal of Turbomachinery*, Vol. 121, No. 1, 1999, pp. 167–174.

[59] Liou, T. M., Chen, M. Y., and Tsai, M. H., "Fluid Flow and Heat Transfer in a Rotating Two-Pass Square Duct with In-Line 90° Ribs," American Society of Mechanical Engineers, ASME Paper GT2001-0185, June 2001.

[60] Liou, T. M., Chen, M. Y., and Wang, Y. M., "Heat Transfer, Fluid Flow, and Pressure Measurements inside a Rotating Duct with Detached 90° Ribs," American Society of Mechanical Engineers, ASME Paper GT2002-30201, June 2002.

[61] Liou, T. M., and Dai, G. Y., "Pressure and Flow Characteristics in a Rotating Two-Pass Square Duct with 45 Deg Angled Ribs," American Society of Mechanical Engineers, ASME Paper GT2003-38346, 2003.

[62] Liou, T. M., Hwang, Y. S., and Li, Y. C., "Flowfield and Pressure Measurements in a Rotating Two-Pass Duct with Staggered Rounded Ribs Skewed 45° to the Flow," American Society of Mechanical Engineers, ASME Paper GT2004-53173, 2004.

[63] Dutta, S., Andrews, M. J., and Han, J. C., "Prediction of Turbulent Flow and Heat Transfer in Rotating Square and Rectangular Smooth Channels," American Society of Mechanical Engineers, ASME Paper 96-GT-234, June 1996.

[64] Stephens, M. A., and Shih, T. I-P., "Computations of Flow and Heat Transfer in a Smooth U-Shaped Square Duct with and without Rotation," *Journal of Propulsion and Power*, Vol. 15, No. 2, 1999, pp. 272–279.

[65] Lin, Y.-L., Shih, T. I-P., Stephens, M. A., and Chyu, M. K., "A Numerical Study of Flow and Heat Transfer in a Smooth and a Ribbed U-Duct with and without Rotation," *Journal of Heat Transfer*, Vol. 123, No. 2, 2001, pp. 219–232.

[66] Bonhoff, B., Tomm, U., Johnson, B. V., and Jennions, I., "Heat Transfer Predictions for Rotating U-Shaped Coolant Channels with Skewed Ribs and Smooth Walls," American Society of Mechanical Engineers, ASME Paper 97-GT-162, 1997.

[67] Sleiti, A. K., and Kapat, J. S., "Effect of Coriolis and Centrifugal Forces on Turbulence and Heat Transfer at High Rotation and Buoyancy Numbers in a Rib-Roughened Internal Cooling Channel," American Society of Mechanical Engineers, ASME Paper GT2004-53018, June 2004.

[68] Iacovides, H., and Raisee, M., "Recent Progress in the Computation of Flow and Heat Transfer in Internal Cooling Passages of Turbine Blades," *International Journal of Heat and Fluid Flow*, Vol. 20, No. 3, 1999, pp. 320–328.

[69] Jang, Y. J., Chen, H. C., and Han, J. C., "Flow and Heat Transfer in a Rotating Square Channel with 45-Degree Angled Ribs by Reynolds Stress Turbulence Model," *Journal of Turbomachinery*, Vol. 123, No. 1, 2001, pp. 124–132.

[70] Al-Qahtani, M., Jang, Y. J., Chen, H. C., and Han, J. C., "Prediction of Flow and Heat Transfer in Rotating Two-Pass Rectangular Channels with 45-Degree Rib Turbulators," American Society of Mechanical Engineers, ASME Paper 2001-GT-187, June 2001; also *Journal of Turbomachinery*, Vol. 124, April 2002, pp. 242–250.

[71] Al-Qahtani, M. S., Chen, H. C., and Han, J. C., "A Numerical Study of Flow and Heat Transfer in Rotating Rectangular Channels ($AR = 4$) with 45-deg Rib Turbulators by Reynolds Stress Turbulence Model," ASME Paper 2002-GT-30216, June 2002.

[72] Jia, R., Saidi, A., and Sunden, B., "Heat Transfer Enhancement in Square Ducts with V-shaped Ribs of Various Angles," American Society of Mechanical Engineers, ASME Paper GT-2002-30209, 2002.

[73] Su, G., Teng, S., Chen, H. C., and Han, J. C., "Computation of Flow and Heat Transfer in Rotating Rectangular Channels ($AR = 4$) with V-shaped Ribs by a Reynolds Stress Turbulence Model," American Society of Mechanical Engineers, ASME Paper GT-2003-38348, June 2003; also *Journal of Thermophysics and Heat Transfer*, Vol. 18, No. 4, 2004, pp. 534–547.

[74] Su, G., Chen, H. C., Han, J. C., and Heidmann, D., "Computation of Flow and Heat Transfer in Rotating Smooth Channels with Several Channel Aspect Ratios by a Reynolds Stress Turbulence Model," *International Journal of Heat and Mass Transfer*, Vol. 47, No. 26, 2004, pp. 5665–5683.

[75] Su, G., Chen, H. C., Han, J. C., and Heidmann, D., "Computation of Flow and Heat Transfer in Two-Pass Rotating Rectangular Channels ($AR = 1{:}1$, $AR = 1{:}2$, $AR = 1{:}4$) with 45-Deg Angled Ribs by Reynolds Stress Turbulence Model," American Society of Mechanical Engineers, ASME Paper GT-2004-53662, June 2004.

[76]Chen, H. C., Jang, Y. J., and Han, J. C., "Computation of Heat Transfer in Rotating Square Channels by a Second-Moment Closure Model," *International Journal of Heat and Mass Transfer*, Vol. 43, No. 9, 2002, pp. 1603–1616.

[77]Chen, H. C., Jang, Y. J., and Han, J. C., "Assessment of a Near-Wall Second-Moment Closure for Rotating Multiple-Pass Cooling Channels," *Journal of Thermophysics and Heat Transfer*, Vol. 14, No. 2, 2000, pp. 201–209.

[78]Chen, H. C., Patel, V. C., and Ju, S., "Solutions of Reynolds-Averaged Navier–Stokes Equations for Three-Dimensional Incompressible Flows," *Journal of Computational Physics*, Vol. 88, No. 2, 1990, pp. 305–336.

[79]Daly, B. J., and Harlow, F. H., "Transport Equations in Turbulence," *Physics of Fluids*, Vol. 13, No. 11, 1970, pp. 2634–2649.

[80]Speziale, C. G., Sarkar, S., and Gatski, T. B., "Modelling the Pressure-Strain Correlation of Turbulence: An Invariant Dynamical Systems Approach," *Journal of Fluid Mechanics*, Vol. 227, 1991, pp. 245–272.

[81]Chen, H. C., "Assessment of a Reynolds Stress Closure Model for Appendage-Hull Junction Flows," *Journal of Fluids Engineering*, Vol. 117, No. 4, 1995, pp. 557–563.

[82]Chen, H. C., "Submarine Flows Studied by Second-Moment Closure," *Journal of Engineering Mechanics*, Vol. 121, No. 10, 1995, pp. 1136–1146.

[83]Bo, T., Iacovides, H., and Launder, B. E., "Developing Buoyancy-Modified Turbulent Flow in Ducts Rotating in Orthogonal Mode," *Journal of Turbomachinery*, Vol. 117, No. 3, 1995, pp. 474–484.

[84]Al-Qahtani, M., Jang, Y. J., Chen, H. C., and Han, J. C., "Flow and Heat Transfer in Rotating Two-Pass Rectangular Channels ($AR = 2$) by Reynolds Stress Turbulence Model," *International Journal of Heat and Mass Transfer*, Vol. 45, No. 9, 2002, pp. 1823–1838.

[85]Jang, Y. J., Chen, H. C., and Han, J. C., "Numerical Prediction of Flow and Heat Transfer in a Two-Pass Square Channel with 90° Ribs," *International Journal of Rotating Machinery*, Vol. 7, No. 3, 2001, pp. 195–208.

[86]Jang, Y. J., Chen, H. C., and Han, J. C., "Computation of Flow and Heat Transfer in Two-Pass Channels with 60° Ribs," *Journal of Heat Transfer*, Vol. 123, No. 3, 2001, pp. 563–575.

[87]Ekkad, S. V., and Han, J. C., "Detailed Heat Transfer Distributions in Two-Pass Square Channels with Rib Turbulators," *International Journal of Heat and Mass Transfer*, Vol. 40, No. 11, 1997, pp. 2525–2537.